Heliyon 9 (2023) e13033

Contents lists available at ScienceDirect

Heliyon

journal homepage: www.cell.com/heliyon

Research article

Role of donors in triggering second order non-linear optical properties of non-fullerene FCO-2FR1 based derivatives: A theoretical perspective

Muhammad Khalid [a,b,*], Mashal Khan [a,b], Iqra Shafiq [a,b], Khalid Mahmood [c], Muhammad Nadeem Akhtar [d], Javed Iqbal [e], Mohammad Khalid Al-Sadoon [f], Wajid Zaman [g], Ataualpa Albert Carmo Braga [h]

[a] *Institute of Chemistry, Khwaja Fareed University of Engineering & Information Technology, Rahim Yar Khan, 64200, Pakistan*
[b] *Centre for Theoretical and Computational Research, Khwaja Fareed University of Engineering & Information Technology, Rahim Yar Khan, 64200, Pakistan*
[c] *Institute of Chemical Sciences, Bahauddin Zakariya University, Multan, 60800, Pakistan*
[d] *Division of Inorganic Chemistry, Institute of Chemistry, Baghdad-ul-Jadeed Campus, The Islamia University of Bahawalpur, Bahawalpur, 63100, Pakistan*
[e] *Department of Chemistry, University of Agriculture, 38000, Faisalabad, Pakistan*
[f] *Department of Zoology, College of Science, King Saud University, PO Box 2455, Riyadh, 11451, Saudi Arabia*
[g] *Department of Life Sciences, Yeungnam University, Gyeongsan, 38541, Republic of Korea*
[h] *Departamento de Química Fundamental, Instituto de Química, Universidade de São Paulo, Av. Prof. Lineu Prestes, 748, São Paulo, 05508-000, Brazil*

ARTICLE INFO

Keywords:
DFT
Second-order NLO response
Density of states
Hyper-polarizability
Non-fullerene

ABSTRACT

The organic compounds are known as an emerging class in the field of nonlinear optical (NLO) materials. In this paper, D–π–A configured oxygen containing organic chromophores (**FD2-FD6**) were designed by incorporating various donors in the chemical structure of **FCO-2FR1**. This work is also inspired by the feasibility of **FCO-2FR1** as an efficient solar cell. Theoretical approach involving DFT functional *i.e.*, B3LYP/6-311G(d,p) was utilized to achieve useful information regarding their electronic, structural, chemical and photonic properties. The structural modifications revealed significant electronic contribution in designing HOMOs and LUMOs for the derivatives with lowered energy gaps. The lowest HOMO-LUMO band gap obtained was 1.223 eV for **FD2** compound in comparison to the reference molecule (**FCO-2FR1**) *i.e.,* 2.053 eV. Moreover, the DFT findings revealed that the end-capped substituents play a key role in enhancing the NLO response of these push-pull chromophores. The UV–Vis spectra of tailored molecules revealed larger λ_{max} values than the reference compound. Furthermore, strong intramolecular interactions showed the highest stabilization energy (28.40 kcal mol^{-1}) for **FD2** in the natural bond orbitals (NBOs) transitions, combined with the least binding energy (-0.432 eV). Successfully, the NLO results were favorable for the same chromophore (**FD2**) which showed the highest value for dipole moment (μ_{tot} = 20.049 *D*) and first hyper-polarizability ($\beta_{tot} = 11.22 \times 10^{-27}$ *esu*). Similarly, the largest value for linear polarizability $\langle\alpha\rangle$ was obtained as 2.936×10^{-22} *esu* for **FD3** compound. Overall, the designed compounds were calculated with greater NLO values as

* Corresponding author. Institute of Chemistry, Khwaja Fareed University of Engineering & Information Technology, Rahim Yar Khan, 64200, Pakistan.;
E-mail addresses: muhammad.khalid@kfueit.edu.pk, Khalid@iq.usp.br (M. Khalid).

https://doi.org/10.1016/j.heliyon.2023.e13033
Received 26 August 2022; Received in revised form 12 January 2023; Accepted 13 January 2023
Available online 17 January 2023

compared to **FCO-2FR1**. The current study may provoke the researchers towards designing of highly efficient NLO materials *via* using the suitable organic linking species.

1. Introduction

From the past few decades, the structural tailoring of advanced materials for obtaining unique non-linear optical (NLO) response has been the most interesting task in the modern research areas. The NLO materials have gained much importance in the advanced research regarding both theoretical and experimental viewpoints. These materials are extremely beneficial in the field of telecommunications [1], optical computing [2], laser technology [3], optoelectronics [4] and photonic devices [5]. Almost all NLO materials have possessed direct relation between optical properties and intensity of incident light [6]. Many schemes have been applied in designing new and improved materials that exhibit excellent NLO response [7]. These materials include; polymer framework; nanomaterials; organic and inorganic semiconductors; organometallic compounds andss molecular dyes [8,9]. Each class shows its own advantages and disadvantages regarding their practical applications for NLO response.

The development in the nonlinear optics focused on the solid inorganic materials such as $LiNbO_3$ and KH_2PO_4 which gradually shifted towards organic and organometallic systems due to various reasons [10]. The transition organometallic complexes also served as potential building blocks for second order NLO materials owing to their low energy and intense electronic charge transfer (CT) excitations [11]. Overtime, novel organic NLO materials have been known as valuable materials for simulation analysis due to their attractive structural features such as, fast reaction chemistry, high hyper-polarizability, low cost, higher band gap and tunable structural modulations to obtain high NLO response. Moreover, they are naturally soft, show high optical transparency and good stability in the visible region [12]. Furthermore, organic materials impart robust NLO response due to the versatility in their molecular structure owning to different functional groups and wide variety of synthetic methodologies. These diverse structural features are the reason that they are extensively being utilized in various optical applications [13] such as frequency doubling, electro-optic switching, modulation, and terahertz (THz) wave production [14].

The rapid intramolecular charge transfer (ICT) has underpinned the NLO properties in organic chromophores generated mainly due to interconnection of strong donor and acceptor moieties *via* the conjugated π-system [15]. A strong D–π–A chromophore can be developed by varying the length and composition of a push-pull system and evaluating the effect of donor-acceptor groups [16]. As NLO response is a property of the entire molecule, therefore the insight of molecular composition is an essential phenomenon. Among various NLO properties, linear polarizability and hyper-polarizabilities have been vital in the proper assessment of NLO response [17].

The non-fullerene based NLO materials have been developed in the recent years and are continuously gaining significant attention nowadays. The non-fullerene acceptors (NFAs) have shown several advantages over their fullerene counterparts such as; low production cost; fine tenability; easy purification; high molar extinction coefficient and strong absorption range in the visible and near infrared (NIR) regions [18]. They have possessed varying electron affinities and chemical structures over a wide range as well as efficient charge separation and small driving energies [19]. Due to these advanced features the efficiency of NFAs has increased dramatically in the recent years. Moreover, NFAs due to their π-conjugated structure provide strong charge transference at donor-acceptor interface in order to facilitate the electronic delocalization [20].

Several useful strategies have been applied in order to develop high performance NFAs such as; increasing extended conjugation; altering π-spacer and insertion of oxygen in the backbone. Among all these strategies, the insertion of oxygen has proved to be the most efficient and useful strategy [21,22]. Recently, some fascinating W-shaped molecules are developed (W1–W6) from the synthesized FCO molecule in order to gain efficient environment friendly solar materials. The toxic –CN group has been replaced with nature friendly electronegative groups ($-CF_3$, $-SO_3H$, $-NO_2$) in the designed chromophores. The materials have shown exceptional photo-physical and photovoltaic properties with lower band gaps as compared to the reference compound and could be efficiently utilized in the future organic solar cells (OSCs) [23].

Our present research work is greatly influenced by the above mentioned compounds and we have planned to design and present a comparative theoretical analysis regarding their electronic, photonic and nonlinear properties. In addition to this, we have also designed some unique molecular geometries from the attractive non-fullerene compound (**FCO-2FR1**) which have not been discussed in the past. It is noteworthy that we have also defined the role of donor species in determining the NLO response of D–π–A configuration in this research regime. **FCO-2FR1** and its designed chromophores (**FD2-FD6**) are extensively analyzed using the most popular density functional methodology which is much better and cost effective technique than other conventional methods 24,25,26,27,28]. The DFT calculations have been used to answer many of the compelling scientific questions which could be impossible to determine *via* experimentation. Moreover, the method is well-suited to optimize the structures once at the initial approximation for the geometry [29].

2. Methodology

The computational calculations for all the designed derivatives were performed *via* Gaussian 09 program [30]. The structures were optimized without any geometrical constrain using the density functional theory (DFT) *i.e.,* B3LYP (Becke, 3-parameter, Lee-Yang-Parr correlation functional) [31] with the basis set such as 6-311G(d,p) [32,33]. Further analysis of the optimized structures was done in order to confirm their real local minima *i.e.,* assuring the absence of imaginary frequencies. For this benchmark study, several bulk-level electronic and optical properties were analyzed using the same DFT functional and basis set approach. These included

density of states (DOS), HOMO-LUMO band gaps, natural bond orbitals (NBOs), global reactivity parameters (GRPs), UV–Visible (UV–Vis) spectroscopy, natural population analysis (NPA), transition density matrix (TDM) and one of the most significant non-linear optical study (NLO). The Gaussview 5.0 software program [34] was utilized to view the optimized geometries. The DOS investigation was performed using PyMOlyze software [35] and revealed the electronic nature of the compounds using energy band gap between HOMOs and LUMOs. Similarly, their stabilization energies were predicted from the NBOs data obtained using NBO program 5.0 [36]. Some other important software programs utilized to interpret the outcomes of various analyses were Avogadro [37], Chemcraft [38] and GaussSum [39]. The global reactivity descriptors (GRDs) included: electron affinity (*EA*), ionization potential (*IP*), electronegativity (X), global softness (σ), electrophilicity index (ω), global hardness (η) and chemical potential (μ) were calculated using Equations (1)–7). The crucial electronic assignments and oscillation frequencies of the studied compounds were examined with the help of UV–Vis spectral data using time dependent DFT (TDDFT). The dipole moment (μ_{tot}) [40], linear polarizability $\langle\alpha\rangle$ [15] and first hyper-polarizability (β_{tot}) [41] values were calculated by using Equations (10)–12). The 3 × 3 tensors for the first hyper-polarizability were calculated through Gaussian suite programs.

3. Results and discussion

3.1. Chemistry of entitled chromophores

The present computational investigation is used to design and interpret promising non-fullerene organic NLO chromophores. For this purpose, we have selected a synthesized oxygen heterocyclic fused NF acceptor molecule as a parent compound (**FCO–2F**). It is based on the A-D-A configuration *i.e.*, central donor moiety surrounded with similar acceptor species at both ends [42]. For the sake of convenience, we have replaced the bulky alkyl (-C_8H_{17}) groups with simple methyl (-CH_3) groups and created a new reference molecule (**FCO-2FR1**) as shown in Fig. 1. The acceptor part is the point of interest as it is having the highly toxic cyano (–CN) groups which must be replaced with some less toxic groups in order to achieve eco-friendly organic non-linear compounds. Moreover, from the literature survey it is cleared that fine tuning of electronic properties greatly depend upon the chemical strength of donors, acceptors and π–spacers incorporated into the structural framework [43]. Therefore, the A moiety at one end is replaced with efficient donors for acquiring D–π–A configuration. Here, the central oxygen containing core unit is playing the role of π–spacer (positively charged) and we have obtained a series of five NF-based eco-friendly NLO compounds (**FD2-FD6**). Fig. 2 shows the colored structures of **FCO-2FR1** and **FD2-FD6** to elaborate the structural differences and their optimized structures are also presented in Fig. S1. The donor moiety incorporated in **FD2** compound is named as *N*-1-(4-(dimethylamino)phenyl)-*N*-4,*N*-4-dimethyl-N-1-phenylbenzene-1, 4-diamine (DPB); in **FD3** as *N*-phenyl-4-(1,3,3a,8b-tetrahydrocyclopenta[*b*]indol-4(2-*H*)-yl)-*N*-(4-(1,3,3a,8b-tetrahydrocyclopenta[*b*] indol-4(2-*H*)-yl)phenyl)aniline (TPA); in **FD4** as *N*-(4-(9-*H*-carbazol-9-yl)phenyl)-4-(9-*H*-carbazol-9-yl)-*N*-phenylaniline (CPA); in **FD5** as *N*-(4-(10-*H*-phenothiazin-10-yl)phenyl)-4-(10-*H*-phenothiazin-10-yl)-*N*-phenylaniline (PPA) and in **FD6** as *N*-(4-(10-*H*-phenoxazin-10-yl)phenyl)-4-(10-*H*-phenoxazin-10-yl)-*N*-phenylaniline (PZA). A schematic representation of all the designed molecules is presented in Fig. 3a. Whereas, Fig. 3b represents the structure of donor species. In order to evaluate how the modification of various donors influence the NLO properties such as dipole moment (μ_{tot}), linear polarizability $\langle\alpha\rangle$ and first-order hyper-polarizability (β_{tot}), the DFT/TDDFT investigation has been performed for the entitled chromophores (**FCO-2FR1** and **FD2-FD6**).

3.2. Electronic properties

The frontier molecular orbitals (FMOs) examination is carried out for pristine reference (**FCO-2FR1**) and newly designed derivatives (**FD2-FD6**) along with their density of states (DOS) analysis. The FMOs are considered as remarkable method for studying the chemical stabilities, electronic transitions and molecular reactivity of organic molecules [44]. Further, the energies of the highest occupied molecular orbitals (HOMOs) and the lowest unoccupied molecular orbitals (LUMOs) of compounds are significant in determining their optical and electronic properties. Concurring to Koopman's hypothesis, HOMO energies with a negative sign explain the ionization potential, while, the LUMO energies demonstrate the electronic affinity of a system [45].

The B3LYP/6-311G(d,p) functional is utilized during FMOs energy calculations, providing a clear understanding of the $E_{HOMO/}$

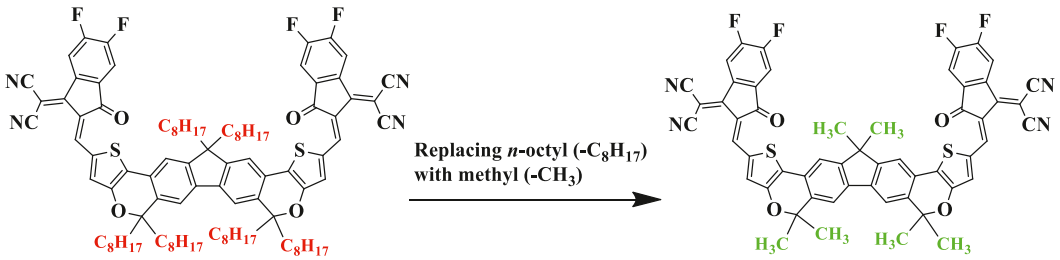

Fig. 1. Side-chain modification of parent molecule **FCO–2F** into a reference **FCO-2FR1.**

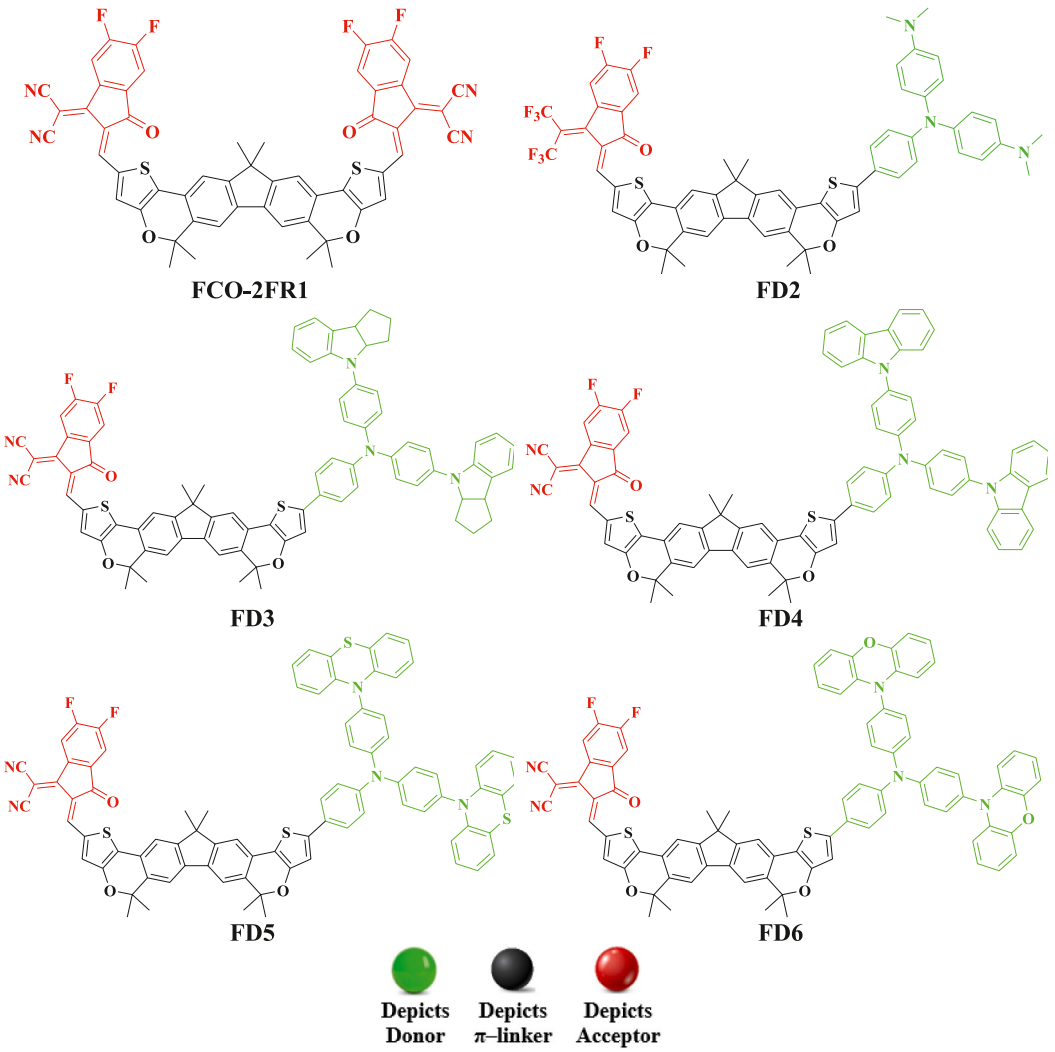

Fig. 2. Structures of reference (**FCO-2FR1**) and designed compounds (**FD2-FD6**).

$_{LUMO}$, representing the E_{gap} in electron volts (*eV*) for the studied compounds (see Table 1). The data obtained for higher energy levels (HOMO-1/LUMO+1 and HOMO-2/LUMO+2) are included in Table S1.

It has been known from the previous studies that compounds with lesser HOMO-LUMO energy gaps are thought to be more reactive, less stable and softer. Consequently, such compounds are considered as better NLO candidates [46]. The theoretically calculated energy values of **FCO-2FR1** (E_{HOMO} = -5.688 and E_{LUMO} = -3.636 eV) are found in close agreement with the experimental results of parent compound, **FCO–2F** [42] (E_{HOMO} = -5.37 eV, E_{LUMO} = -3.78 eV with Δ E = 1.59 eV).

The HOMO-LUMO energy gap found in **FCO-2FR1** is 2.053 eV and the doping of compound with donors increased the energy of HOMO orbitals in the derivatives (**FD2-FD6**). Excessive electronic flow due to structural modification caused the formation of new HOMOs and consequently, the electrons reside in them and efficiently travel towards new LUMOs.

The E_{HOMO} values observed for **FD2-FD6** are -4.659, -4.754, -5.189, -5.239, and -5.069 eV, respectively. Similarly, E_{LUMO} calculated as -3.436, -3.446, -3.464, -3.465, and -3.468 eV, respectively. In comparison to **FCO-2FR1**, quite high HOMO energies are observed in the designed compound implying that HOMOs are formed at higher position than the reference molecule. The ultimate band gap is narrowed in all the designed molecules (**FD2-FD6**) allowing for a high charge transfer rate between their molecular orbitals.

The lowest energy gap value observed in the **FD2** (1.223 eV) is most likely due to the efficient donor (DPB) end-capped group. In case of **FD3**, the energy gap is found to be smaller than **FCO-2FR1**, but greater than **FD2** (1.308 > 1.223 eV) which might be due to the lesser resonance effect in its donor moiety (TPA). Furthermore, the lower HOMO-LUMO band gap are observed in **FD6** (1.601 eV) due to the presence of heteroatom (O-atom) in its donor part (PZA) which enhances the electron transfer process and lowers the energy gap. The other compounds like **FD4** and **FD5** showed higher band gaps than **FD6** (1.725 and 1.774 eV, respectively). The overall increasing order of HOMO-LUMO band gaps for the investigated molecules is as follows: **FD2 < FD3 < FD6 < FD4 < FD5 < FCO-2FR1**.

A comparative analysis of various donors determined that the most effective push-pull mechanism is found in **FD2** and **FD3** with

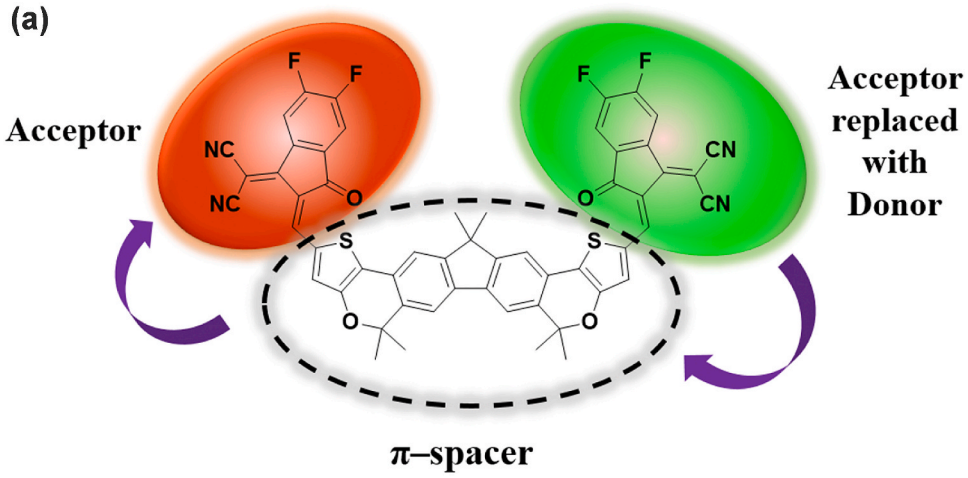

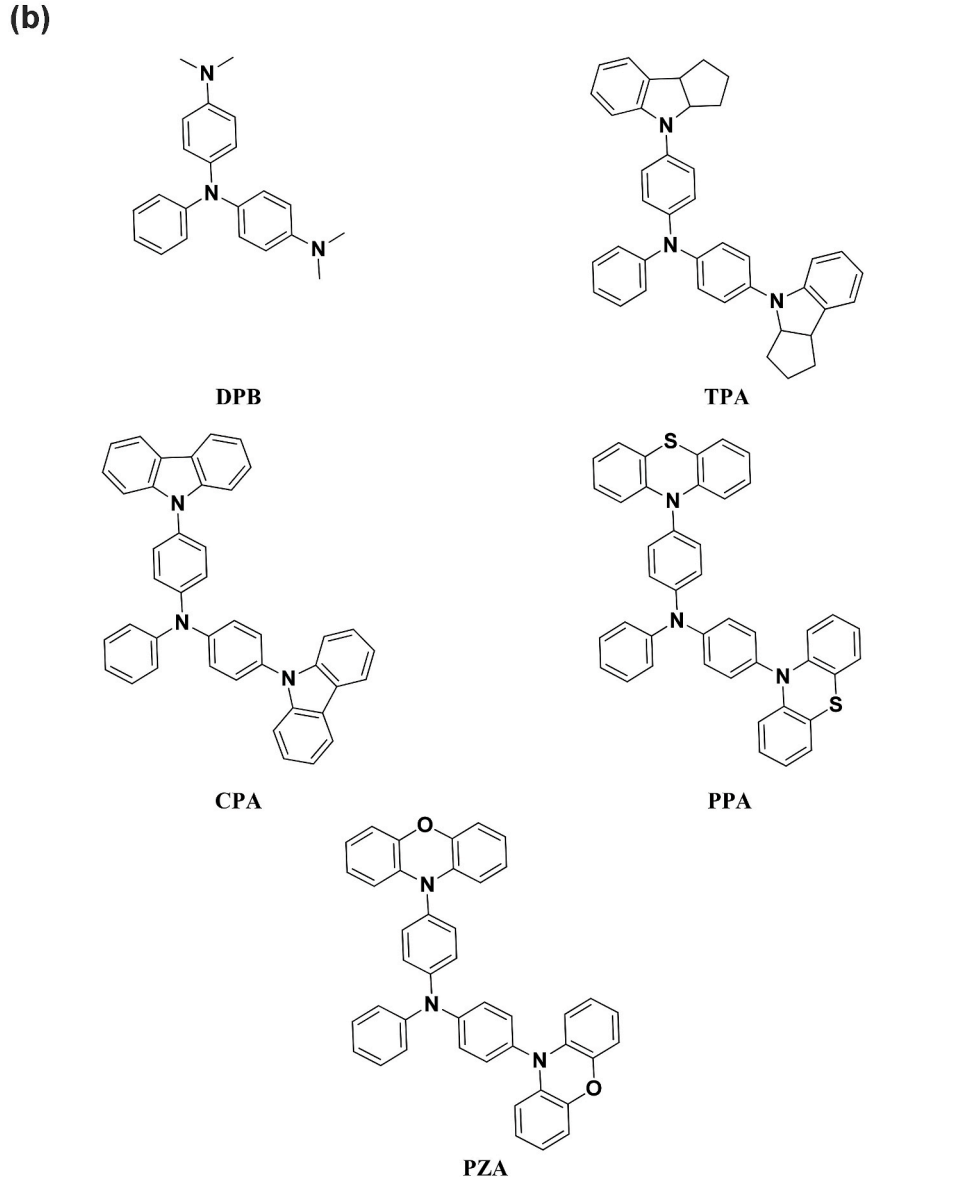

(caption on next page)

Fig. 3a. Schematic representation of reference and various donors used in the designed chromophores.
Fig. 3b: The structures of various donor moieties used in the designed compounds (FD2-FD3).

Table 1
Calculated energy (E_{HOMO}/E_{LUMO}) and energy gap (ΔE) of the entitled compounds in *eV*.

Compounds	E_{HOMO}	E_{LUMO}	E_{gap}
FCO-2FR1	-5.688	-3.635	2.053
FD2	-4.659	-3.436	1.223
FD3	-4.754	-3.446	1.308
FD4	-5.189	-3.464	1.725
FD5	-5.239	-3.465	1.774
FD6	-5.069	-3.468	1.601

DPB and TPA donors incorporated, respectively. Both the donor species are enriched in electrons for donation hence, create a strong intramolecular transfer of electrons with lesser HOMO-LUMO band gaps in D-π-A systems. On the other hand, the distinct chemical frameworks and less efficient push-pull mechanism exhibited larger band gaps in case of **FD4**, **FD5** and **FD6** having CPA, PPA and PZA donor groups, respectively.

The obtained results clearly demonstrate that the structural tailoring by introducing various electron-rich donor substituents is a suitable way to improve the NLO response. Moreover, the lesser energy gap values explained the sufficient intramolecular charge transfer (ICT) within these π-conjugated molecule which is an evidence of the NLO materials' functionality [47].

3.3. Density of states (DOS)

The DOS outcomes corroborated the results shown in the FMOs diagrams and explain the electronic distribution in boundary molecular orbitals [48]. Fig. 4 demonstrates HOMOs and LUMOs of **FCO-2FR1** and **FD2-FD6** which clearly depict the electronic re-distribution pattern in the studied compounds by altering electron donors at their terminal portion. However, the HOMO-1/-LUMO+1 and HOMO-2/LUMO+2 of the above mentioned compounds are also represented in Fig. S2. The electronic density in case of **FCO-2FR1** at HOMO is present mostly in the central core of the molecule and minutely on the terminal acceptors (A-D-A). While, in case of LUMO, the entire molecule is covered with the electronic clouds. In **FD2**, **FD3** and **FD6** compounds, the donor region shows the clear electronic charge density at HOMO while, even distribution of charge is seen at the acceptor region and minutely at the central π–spacer in their LUMOs according to the trend (see Fig. 4). However, different distribution pattern is observed at HOMOs of other designed derivatives (**FD4** and **FD5**). In this case, a great extent of electronic charge is also observed at central π–spacer region and minutely at the donor region, while, the same trend is followed in their LUMOs as described previously *i.e.*, acceptor region is showing the electron density.

DOS pictographs are used to understand the participation of each molecular fragment in determining the electronic characteristics of the studied molecules. The interpretation was performed at the same DFT functional for **FCO-2FR1** and **FD2-FD6**. For determining the total density of states (TDOS), we split our studied molecules into separate fragments. The **FCO-2FR1** is divided into two fragments *i.e.*, donor (D) and acceptor (A) while, the derivative compounds (**FD2-FD6**) are divided into three segments *i.e.*, donor, π-spacer and acceptor. The pictographs of all the examined compounds are shown in Fig. 5.

Herein, the donor shows contribution as 76.7% to HOMO and 35.7% to LUMO, while contribution of acceptor is 23.3% to HOMO and 64.3% to LUMO for **FCO-2FR1**. However, for **FD2-FD6** the participation of donor is 84.2, 86.9, 46.3, 32.8, 100% to HOMO and 0.4, 0.4, 0.3, 0.3 and 0.3% to LUMO, respectively. Similarly, π-spacer contributes 15.2, 11.9, 50.7, 63.1, 0.0% to HOMO and 33.8, 33.1, 33.4, 33.4, 33.4% to LUMO in **FD2-FD6**, correspondingly. Likewise, acceptor demonstrated the electronic distribution pattern as 0.7, 1.2, 3.0, 4.1, 0.0% to HOMO, while, 65.7, 66.5, 66.3, 66.3 and 66.4% to LUMO for **FD2-FD6**, respectively. The given data shows that in case of **FCO-2FR1**, **FD2**, **FD3** and **FD6** the HOMO is concentrated on donor, while, in case of **FD4** and **FD5**, it is majorly resided over the π-spacer. Similarly, the relative density of LUMO is more intense over the acceptor region in all the studied compounds (see Fig. 5). The overall contribution pattern illustrates a considerable electronic charge variation in molecular systems which depicts that a significant amount of charge transfer takes place from the donor to acceptor region *via* the π-spacer.

3.4. The UV–vis analysis

In an attempt to interpret the probability of charge transfer, electronic excitation energy, maximum absorption and oscillation frequency within the studied compounds, UV–Vis spectral analysis is performed using time dependent DFT functional *i.e.*, B3LYP/6-311G(d,p). The afore-mentioned parameters are calculated in both gas and solvent (chloroform) phases, as summarized in Table 2. While, the six lowest singlet-singlet transitions are recorded in Tables S2–S13.

The conductor like polarizable continuum model (CPCM) [49] is employed for calculating the absorption spectra in the chloroform solvent in order to achieve better comprehension of optical properties of systems. Moreover, the polar medium involved the π→π* and n→π* stabilization state at suitable energy level [50]. It has been mainly observed that the UV–Vis data obtained for a polar medium is highly influenced by the van der Waals interactions. More specifically, hydrogen bonding and dipole forces significantly enhance the stabilization of the first singlet transition level of systems under investigation. The greater polarity in the excited states as compared to

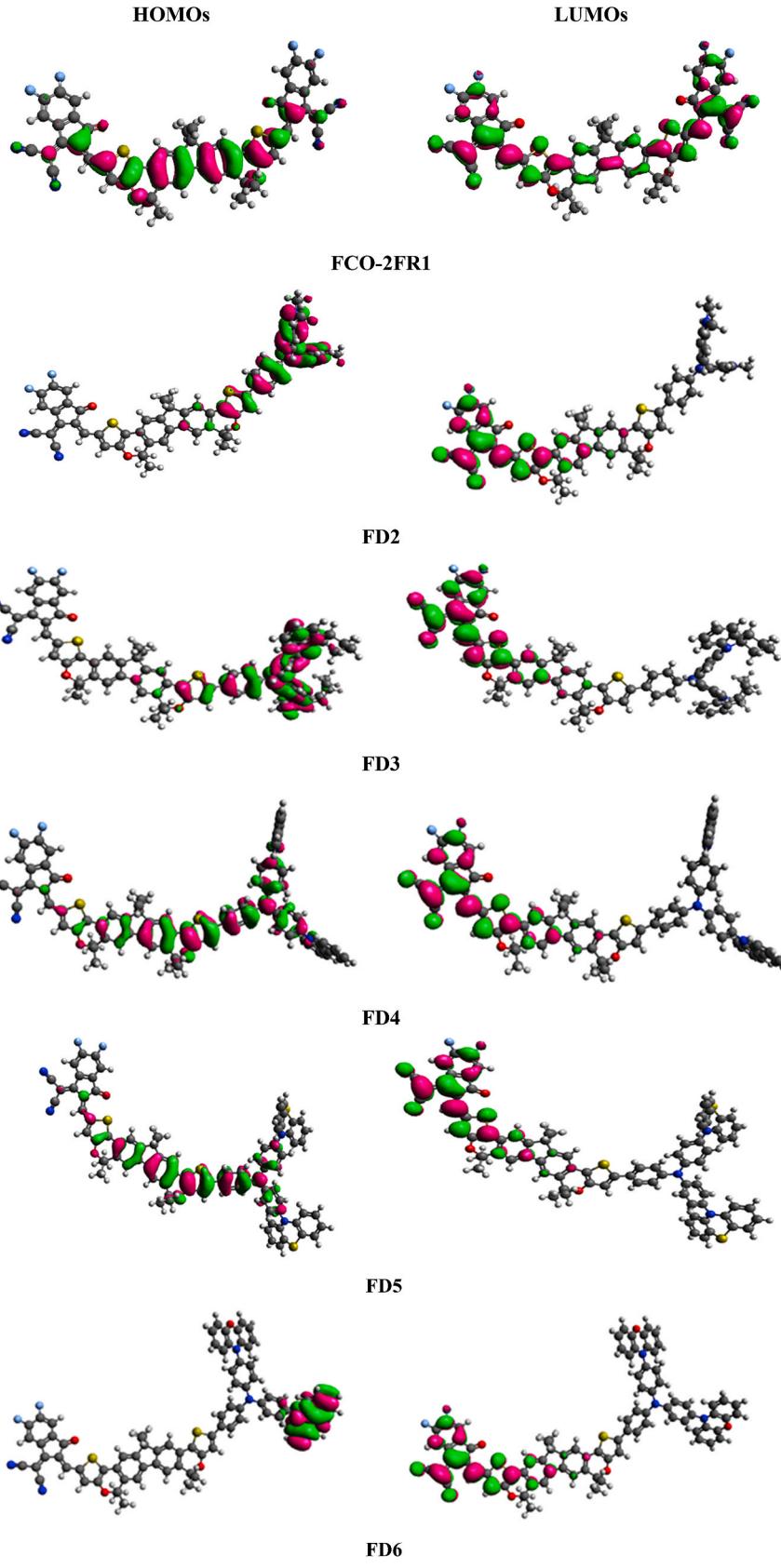

(caption on next page)

Fig. 4. HOMOs and LUMOs of entitled compounds (**FCO-2FR1** and **FD2-FD6**).

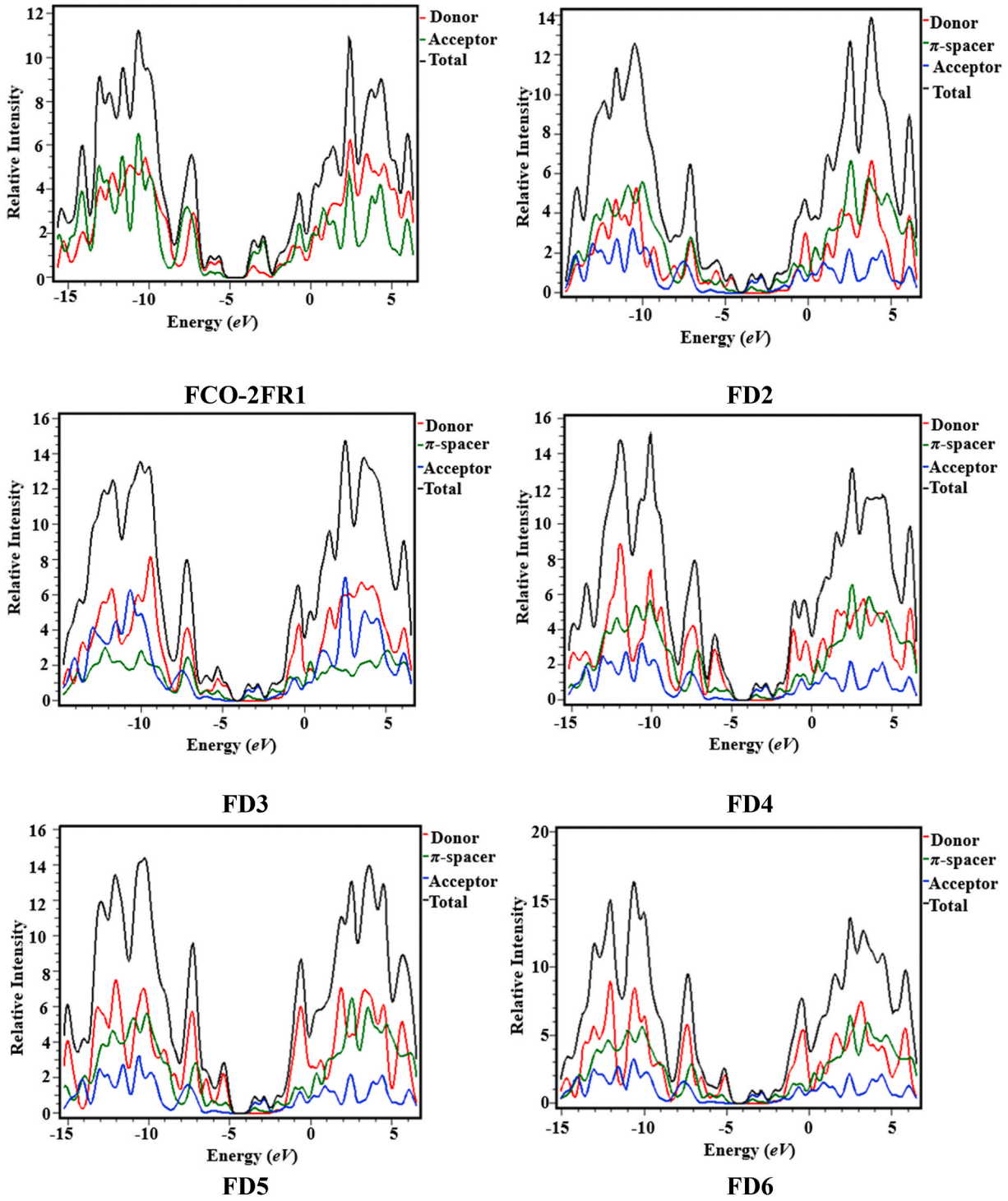

Fig. 5. Graphical representation of density of states for **FCO-2FR1** and **FD2-FD6**.

Table 2
Computed transition energies (*eV*), maximum absorption wavelengths (*nm*), oscillator strengths (f_{os}) and transition natures of designed compounds in solvent phase and gaseous phase.

	Systems	DFT λ_{max}	EXP λ_{max}	*E*	f_{os}	MO contributions
Solvent Phase (Chloroform)	**FCO-2FR1**	711.408	703	1.743	2.176	H→L (98%)
	FD2	749.059	–	1.655	0.919	H-1→L (77%)
	FD3	752.697	–	1.647	0.904	H-1→L (68%)
	FD4	810.725	–	1.529	0.851	H→L (98%)
	FD5	792.738	–	1.564	0.974	H→L (99%)
	FD6	784.760	–	1.580	0.990	H-2→L (99%)
Gaseous Phase	**FCO-2FR1**	659.210	–	1.881	1.956	H→L (99%)
	FD2	542.672	–	2.285	1.029	H-3→L (69%)
	FD3	714.647	–	1.735	0.725	H-1→L (97%)
	FD4	751.738	–	1.649	0.685	H→L (99%)
	FD5	728.719	–	1.701	0.693	H-2→L (73%)
	FD6	718.749	–	1.725	0.882	H-2→L (99%)

ground level induces the electronic transitions towards longer wavelength (bathochromic shift) [51]. Table 2 clearly shows that all the compounds exhibited maximum absorption wavelengths in the visible region of electromagnetic spectrum.

The theoretical value of λ_{max} for **FCO-2FR1** (in chloroform solvent) shows a great correspondence with experimental value of parent compound (**FCO–2F**) [42] *i.e.*, 711.408 and 703 nm. Moreover, the corresponding energy of transition calculated for **FCO-2FR1** is 1.743 eV, the oscillation frequency (f_{os}) is 2.176 and the major orbital assignment is H→L (98%). All the designed chromophores show a red-shift with higher λ_{max} values as compared to **FCO-2FR1**. The highest value is obtained for compound **FD4** (810.725 nm) as compared to other derivatives. Therefore, it is regarded as a compound with the largest bathochromic shift which might be due to its unique chemical framework. The following order of UV–Vis wavelengths (*nm*) is seen in the compounds under analysis: **FCO-2FR1** (711.408) < **FD2** (749.05) < **FD3** (752.697) < **FD6** (784.760) < **FD5** (792.738) < **FD4** (810.725). Similarly, their corresponding transition energies (*eV*) are found in the reverse order of the wavelengths as: **FCO-2FR1** (1.743) > **FD2** (1.655) > **FD3** (1.647) > **FD6** (1.580) > **FD5** (1.564) > **FD4** (1.529). The oscillation frequencies are as follows: **FCO-2FR1** = 2.176, **FD2** = 0.919, **FD3** = 0.904, **FD4** = 0.851, **FD5** = 0.974 and **FD6** = 0.990. Among designed molecules, 99% molecular orbital transition is seen in first transition energy levels such as: H→L in case of **FD5**. While, in compounds **FD2**, **FD3**, **FD4** and **FD6**, the major orbital transitions seen are: H-1→L (77%), H-1→L (68%), H→L (98%) and H-2→L (99%), accordingly.

In gaseous phase, the reference **FCO-2FR1** showed the λ_{max} = 659.210 nm with major HOMO-LUMO contributions observed as H→L (99%) and an oscillation frequency (f_{os}) of 1.956. Except for **FD2**, all the designed compounds (**FD3-FD6**) exhibited higher λ_{max} values than **FCO-2FR1** in the range of 714.647–751.738 nm. A blue-shift is seen in case of **FD2** with 542.672 nm as λ_{max} and a higher transition energy of 2.285 eV (higher than **FCO-2FR1**) with an oscillation strength of 1.029. Whereas, in case of **FD3**, a significantly higher λ_{max} value is obtained as 714.647 nm and less transition energy of 1.735 eV. The frequency of oscillation in compound is calculated to be 0.725 showing major molecular orbital contributions from H-3→L as 69%. Similarly, the compound **FD4** showed the highest absorption wavelength as 751.738 nm and lowest energy of transition as 1.649 eV with a least oscillation frequency of 0.685 (see Table 2). The other derivatives (**FD5** and **FD6**) showed λ_{max} values as 728.719 and 718.749 nm with corresponding energies as 1.701 and 1.725 eV, respectively. The percentages of major molecular orbital contributions are observed as 73 and 99% for similar level (H-2→L) in both compounds with an oscillation frequency of 0.693 and 0.882, accordingly.

In gas phase, the maximum absorption wavelengths (λ_{max}) of all molecules are discovered to be in the following increasing order:

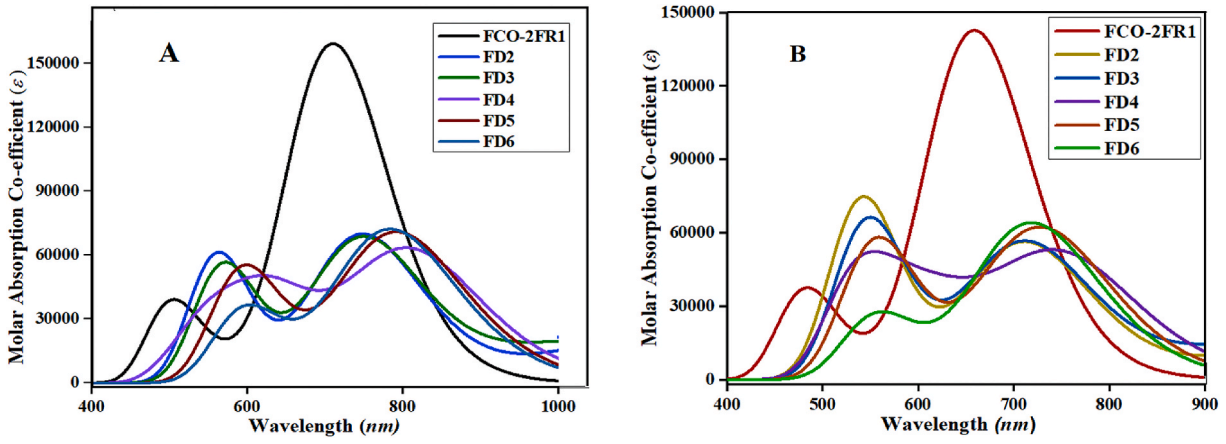

Fig. 6. UV–Vis plots for **FCO-2FR1** and **FD2-FD6** in chloroform solvent (A) and gas phase (B).

FD2 < FCO-2FR1 < FD3 < FD6 < FD5 < FD4. Excitation energy is another method for measuring the efficiency of NLO material. In general, lower molecular excitation energy provides higher power conversion efficiency. The molecular transition energies are observed in the reverse order as: **FD2 > FCO-2FR1 > FD3 > FD6 > FD5 > FD4**. The oscillator strengths of the investigated compounds are found in the same order as the energy of transition. The UV–Vis plots in both solvent (chloroform) and gaseous phase are demonstrated in Fig. 6 (A and B, respectively).

Concisely, the doping of reference compound with suitable donors resulted in clear red-shift in case of the designed compounds. The lower excitation energy and large charge transfer in molecular orbitals demonstrated that these molecules are promising candidates for best use in various NLO applications.

3.5. Global reactivity parameters (GRPs)

The malleability and stability of the studied compounds (**FCO-2FR1** and **FD2-FD6**) are mainly predicted by working on their global reactivity parameters as defined by Koopmans' theorem [52]. The electron donating and accepting properties of molecules in a chemical system are directly related to the ionization potential (*IP*) and electron affinity (*EA*), respectively. The other important parameter is electronegativity (*X*) [53] which determines the potential of a molecule to attract the electronic cloud towards itself. Moreover, parameters like *IP* and *X* play a significant role in determining the reactivity and stability patterns of the studied organic species. Furthermore, the negative values of chemical potential (μ) depict a clear picture of stability for the organic compounds which resist towards their decomposition. The electrophilicity index (ω) [54] describes the energy variations in correlation with the maximum amount of electronic charge transferred. The other global reactivity descriptors including chemical hardness (η) [55,56] and softness (σ). Equations (1)–7) are used to estimate the GRPs which are mentioned here;

$$IP = -E_{HOMO} \quad \text{(Equation 1)}$$

$$EA = -E_{LUMO} \quad \text{(Equation 2)}$$

$$\mu = -\frac{(IP + EA)}{2} \quad \text{(Equation 3)}$$

$$X = \frac{[IP + EA]}{2} \quad \text{(Equation 4)}$$

$$\eta = \frac{(IP - EA)}{2} \quad \text{(Equation 5)}$$

$$\sigma = \frac{1}{(IP - EA)} \quad \text{(Equation 6)}$$

$$\omega = \frac{\mu^2}{2\eta} \quad \text{(Equation 7)}$$

The GRP values are depicted for **FCO-2FR1** and **FD2-FD6** and are shown in Table 3.

The results predict some very important facts about HOMO-LUMO band gaps and various global reactivity parameters. A close relationship is found between GRPs and energy gaps. Greater the energy band gap between HOMO and LUMO, the more is the kinetic stability of a molecule with resistance towards change in electronic configuration [57]. The enhanced stability results into harder molecules with the least reactivity. Contrarily, the compounds having small energy gaps are softer, having flexible character, greater reactivity and less kinetic and physical stability. Hence, the lesser energy gap marked suitable NLO materials with higher polarizabilities.

The stability and reactivity of investigated compounds are quantified by utilizing the energy values of their FMOs [58]. Overall, the ionization potential values for **FCO-2FR1** and **FD2-FD6** are observed to be larger as compared to their electron affinity values describing the better electron donating capability of molecules. Among the designed compounds, the maximum *IP* value is found as 5.239 eV in case of **FD5**, while, the minimum value is observed in **FD2** compound as 4.659 eV. The decreasing order of ionization potential is observed to be: **FCO-2FR1 > FD5 > FD4 > FD6 > FD3 > FD2**. The highest electron affinity (*EA*) value is calculated as

Table 3
Global reactivity parameters for **FCO-2FR1** and **FD2-FD6** in *eV*.

Compounds	*IP*	*EA*	*X*	η	μ	ω	σ
FCO-2FR1	5.688	3.635	4.662	1.027	-4.662	10.584	0.487
FD2	4.659	3.436	4.048	0.612	-4.048	13.395	0.817
FD3	4.754	3.445	4.100	0.654	-4.100	12.851	0.765
FD4	5.189	3.464	4.327	0.863	-4.327	10.851	0.580
FD5	5.239	3.465	4.352	0.887	-4.352	10.676	0.563
FD6	5.069	3.468	4.269	0.801	-4.269	11.380	0.624

3.468 eV in **FD6**, while, 3.436 eV is the least value observed in compound (**FD2**).

Chemical potential (μ) is another parameter to study the reactivity and stability of compounds under investigation. It varies inversely with reactivity of compounds and directly with the stability. The more negative μ values predict the more reactivity and less stability of a D-π-A system [59]. Table 3 shows the negative chemical potential for derivatives (**FD2-FD6**). Moreover, the calculated hardness values are presented in the following decreasing order: **FCO-2FR1 > FD5 > FD4 > FD6 > FD3 > FD2**, which follows exactly the same trend as followed by E_{gap} values. Nevertheless, the chemical hardness (η) values (in *eV*) are greater for **FD5** (0.887) in comparison to **FD2** (0.612), **FD3** (0.654), **FD4** (0.863) and **FD6** (0.801), which certainly reflected more stability of **FD5** compound as compared to the other derivatives. The order of increasing softness is as follows: **FCO-2FR1 < FD5 < FD4 < FD6 < FD3 < FD2** which is the reverse of hardness order. The global electrophilicity (ω) of studied compounds are found in the following decreasing order: **FD2 > FD3 > FD6 > FD4 > FD5 > FCO-2FR1**.

Due to the existence of strong donor species, more electron donating tendency is found among the designed molecules. The statement is valid for the designed chromophores which have shown effective CT potential among their HOMOs and LUMOs. The compound (**FD2**) is predicted as the most favorable fabricated molecule among all, owing to its highest value of softness (0.817 eV) and the lowest hardness (0.612 eV) which coincide with its lowest energy gap (1.223 eV).

3.6. Natural bond orbitals (NBOs) study

NBOs investigation gives an extensive approach relating to charge density transference and intramolecular charge delocalization from filled donor (D) orbitals towards vacant acceptor (A) orbitals in the π-conjugated framework [60]. It is also efficient in elucidating local orbital interactions between bonds as well as hyper-conjugative interactions between the electrophile and nucleophile. Second order perturbation approach [61] helps in analyzing the delocalization reactions, utilizing the following Equation (8):

$$E^{(2)} = q_i \frac{\left(F_{i,j}\right)^2}{\varepsilon_j - \varepsilon_i} \quad \text{(Equation 8)}$$

Here, i and j corresponds to D and A motifs, respectively, $E^{(2)}$ is stabilization energy following i → j delocalization. Moreover, q_i, $F_{i,j}$ and $\varepsilon_j - \varepsilon_i$ are donor orbital occupancy, diagonal and off-diagonal NBO fock matrix elements [62].

Literature conveys the information about NBOs charges for individual D, π-spacer and A species that the positive charges are regarded to donor motif, negative charges to the acceptor while, π-linkers show both (positive and negative) charges based on their molecular framework. Positive charge of π-conjugated linker characterizes that they avoid electron trapping thus facilitating smooth transference of electrons. The calculation of NBO charges conveys information about the net charge transfer within the systems under investigation. Table 4 depicts the natural charges for entitled molecules (**FCO-2FR1** and **FD2-FD6**). The calculations show that all the designed compounds including reference exhibit same trend of electronic charges. The D and π-linker possess positive charges while, the A species attain negative charges. The derivative **FD2** is nominated with the most successful ICT because of the most positively charge donor **(DPB)** and 2-(5,6-difluoro-3-oxo-2,3-dihydro-1-*H*-inden-1-ylidene)malononitrile as acceptor species incorporated into its molecular structure (see Table 4). Similarly, after **FD2**, **FD3** is nominated as a molecule with favorable CT, owing to the efficiency of utilized donor units. These results elucidate successful charge transfer from D towards A without any charge trapping in π-linker leaded to the formation of charge separation state.

Intramolecular transitions result in system's stabilization are σ → σ*, π → π*, LP → σ* and LP → π*. Moreover, the charge transference in π → π* are dominant than σ → σ* transitions. Table 5 predicts the most important selected transitions for the investigated compounds, while, the detailed NBOs values are recorded in Tables S14–S19. The interactions are among the local orbitals which included both occupied bonding and empty non-bonding orbitals.

In **FCO-2FR1**, the significant values of stabilization energy (E^2) obtained are 27.31, 9.82, 63.05 and 20.25 kcal mol^{-1} correspond to transitions among π(C21–C22) → π*(C24–C25), σ(C24–H60) → σ*(S20–C22), LP2 (O54) → σ*(C26–C28) and LP(1)(O2) → π*(C1–C6), respectively. The lowest stabilization energies in π(C68–N69) → π*(C70–N71) and σ(C74–C84) → σ*(C84–H85) are recorded as 0.79 and 0.57 kcal mol^{-1}, respectively.

For derivative **FD2**, the highest π → π* transition energy is obtained among all the derived values for this transition *i.e.,* 28.40 kcal mol^{-1} obtained for π(C27–C28) → π*(C30–C31) transitions. The lowest value is 3.9 kcal mol^{-1} for π(C32–O45) → π*(C30–C31). The feeble σ → σ* transitions also show significant values calculated as 9.99 and 0.58 kcal mol^{-1} regarded as the highest and the lowest values, for σ(C30–H42) → σ*(S26–C28) and σ(C9–C55) → σ*(C55–H57), correspondingly. The transitions due to resonance involving lone pair of electrons also play an important role in determining the chemical nature and electronic transition patterns in compound.

Table 4
Natural charges for donor (D), π-spacer and acceptor (A) moieties for the investigated systems.

Compounds	Donor	π-linker	Acceptor
FCO-2FR1	0.530098	–	-0.38537
FD2	0.13985	0.092451	-0.2323
FD3	0.120001	0.107683	-0.2277
FD4	0.090669	0.130653	-0.22132
FD5	0.087627	0.133047	-0.22068
FD6	0.084235	0.135728	-0.21996

Table 5
Selective natural bond orbitals (NBOs) of investigated compounds (**FCO-2FR1** and **FD2-FD6**).

Compounds	Donor(*i*)	Type	Acceptor(*j*)	Type	$E^{(2)}$	F(i,j)[c]	$E(J)E(i)$[b]
FCO-2FR1	C21–C22	π	C24–C25	π*	27.31	0.30	0.081
	C68–N69	π	C70–N71	π*	0.79	0.45	0.017
	C24–H60	σ	S20–C22	σ*	9.82	0.71	0.075
	C74–C84	σ	C84–H85	σ*	0.57	1.03	0.022
	O2	LP(1)	C1–C6	π*	63.05	0.15	0.106
	O54	LP(2)	C26–C28	σ*	20.25	0.72	0.109
FD2	C27–C28	π	C30–C31	π*	28.40	0.29	0.082
	C32–O45	π	C30–C31	π*	3.90	0.41	0.038
	C30–H42	σ	S26–C28	σ*	9.99	0.71	0.075
	C9–C55	σ	C55–H57	σ*	0.58	1.01	0.022
	N110	LP(1)	C93–C97	π*	41.33	0.27	0.099
	O45	LP(2)	C32–C34	σ*	20.28	0.72	0.109
FD3	C27–C28	π	C30–C31	π*	28.27	0.29	0.082
	C47–N48	π	C49–N50	π*	0.80	0.45	0.017
	C30–H42	σ	S26–C28	σ*	9.97	0.71	0.075
	C124–C125	σ	C125–H132	σ*	0.50	1.01	0.02
	N110	LP(1)	C135–C136	π*	40.67	0.28	0.098
	O45	LP(2)	C32–C34	σ*	20.28	0.72	0.109
FD4	C27–C28	π	C30–C31	π*	28.08	0.29	0.082
	C49–N50	π	C47–N48	π*	0.81	0.44	0.017
	C30–H42	σ	S26–C28	σ*	9.93	0.71	0.075
	C54–C75	σ	C12–C13	σ*	0.50	1.16	0.022
	N110	LP(1)	C122–C123	π*	39.55	0.29	0.097
	O45	LP(2)	C32–C34	σ*	20.28	0.72	0.109
FD5	C27–C28	π	C30–C31	π*	28.06	0.29	0.082
	C32–O45	π	C34–C36	π*	4.40	0.40	0.041
	C30–H42	σ	S26–C28	σ*	9.92	0.71	0.075
	C143–S152	σ	C142–C143	σ*	0.50	1.21	0.022
	O52	LP(2)	C18–C19	π*	30.05	0.34	0.097
	O45	LP(2)	C32–C34	σ*	20.27	0.72	0.109
FD6	C27–C28	π	C30–C31	π*	28.05	0.29	0.081
	C49–N50	π	C47–N48	π*	0.81	0.44	0.017
	C30–H42	σ	S26–C28	σ*	9.92	0.71	0.075
	C54–C75	σ	C12–C13	σ*	0.50	1.16	0.022
	N110	LP(1)	C122–C123	π*	36.43	0.28	0.093
	O45	LP(2)	C32–C34	σ*	20.27	0.72	0.109

Among lone pair transitions LP1(N110) → π*(C93–C97) and LP2(O45) → σ*(C32–C34) are the most significant transitions recorded with energy values as 41.33 and 20.28 kcal mol^{-1}, respectively.

The stabilization energy values in case of **FD3** are recorded as 28.27, 0.80, 9.97, 0.50, 40.67 and 20.28 kcal mol^{-1} with relative transitions as π(C27–C28) → π*(C30–C31), π(C47–N48) → π*(C49–N50), σ(C30–H42) → σ*(S26–C28), σ(C124–C125) → σ*(C125–H132), LP1(N110) → π*(C135–C136), LP2(O45) → σ*(C32–C34), respectively. The compound **FD3** is regarded as a significant chromophore and shows second highest values for π-conjugated transitions after **FD2**.

In **FD4**, the transitions like π(C27–C28) → π*(C30–C31), σ(C30–H42) → σ*(S26–C28) and LP(1)(N110) → π*(C122–C123) are obtained with the highest values as 28.08, 9.93 and 39.55 kcal mol^{-1}, respectively. Similarly, the smallest stabilization energy values for the above mentioned transitions in **FD4** are found as 0.81, 0.50 and 20.28 kcal mol^{-1} observed in due to the π(C49–N50) → π*(C47–N48), σ(C54–C75) → σ*(C12–C13) and LP(2)(O45) → σ*(C32–C34) transitions, correspondingly.

For **FD5**, the highest value of stabilization energy for π → π* transition energy is obtained for π(C27–C28) → π*(C30–C31) as 28.06 kcal mol^{-1}. Among weaker σ → σ* transitions, σ(C30–H42) → σ*(S26–C28) are the most prominent with largest value for compound *i.e.*, 9.92 kcal mol^{-1}. Similarly, LP(2)(O52) → π*(C18–C19) are obtained with stabilization energy as 30.05 kcal mol^{-1} is the highest lone pair transition for **FD5**. The lowest corresponding transitions are π(C32–O45) → π*(C34–C36), σ(C143–S152) → σ*(C142–C143) and LP(2)(O45) → σ*(C32–C34) with respective energy values as 4.4, 0.50 and 20.27 kcal mol^{-1}, respectively.

The **FD6** is the last derivative in which, π(C27–C28) → π*(C30–C31), σ(C30–H42) → σ*(S26–C28) and LP(1)(N110) → π*(C122–C123) transitiond are recorded with highest value of $E^{(2)}$ as 28.05, 9.92 and 36.43 kcal mol^{-1}, respectively. While, the lowest $E^{(2)}$ value is recorded for the transitions like; π(C49–N50) → π*(C47–N48), σ(C54–C75) → σ*(C12–C13) and LP(2)(O45) → σ*(C32–C34) at 0.81, 0.5 and 20.27 kcal mol^{-1}, respectively.

It is evident from the above discussion that the NBOs results of all the studied compounds are closely related to each other. However, the highest stabilization energies are obtained for **FD2** as compared to other designed compounds. This might be due to the presence of efficient end-capped donor moiety (DPB). The NBO charges also support the molecular stability of compound. Hence, it is proved that intramolecular charge transfer (ICT) and hyper-conjugation highly influence the stabilization of investigated molecules and are the main cause to their exclusive NLO properties.

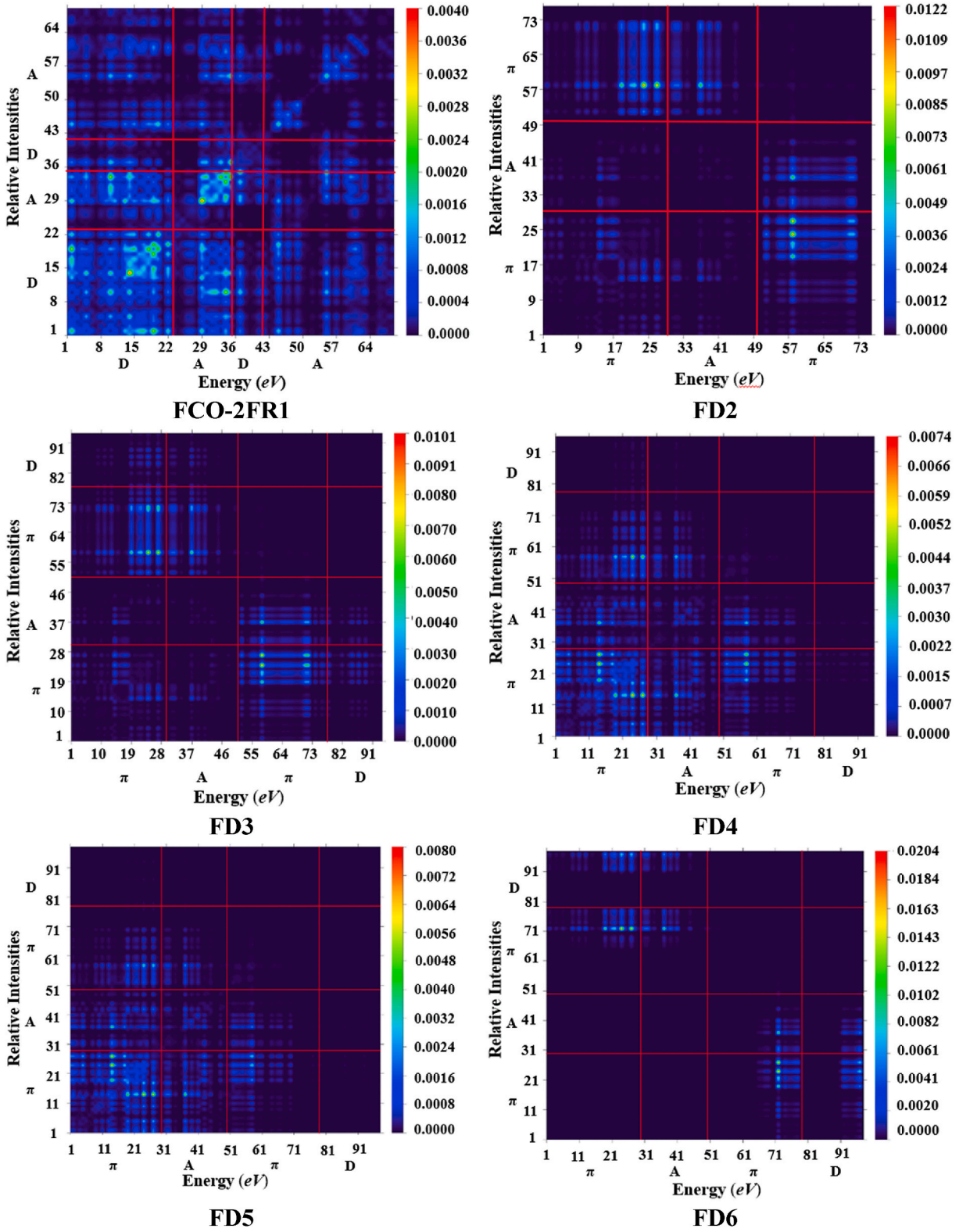

Fig. 7. TDM heat maps for the entitled chromophores (**FCO-2FR1** and **FD2-FD6**).

3.7. Transition density matrices (TDMs)

The electronic excitation phenomena in the newly designed chromophores (**FD2-FD6**) are interpreted efficiently by TDM graphs and compared with the reference compound (**FCO-2FR1**) [63,64]. With use of the Multiwfn 3.8 program [65], we have interpreted the coherence of electronic excitations in the individual fragments of each molecule *i.e.*, donor, π-linker and acceptor. We have neglected the effect of H-atoms due to their least contributions in the transitions of our interest. Fig. 7 displays the TDM heat maps which depict the pattern of flow of electrons in the form of colored spots. In reference compound (**FCO-2FR1**), an efficient diagonal electronic delocalization occurs from D towards A region. However, in the designed molecules (**FD2-FD6**), the charge density is most efficiently transferred in **FD4** and **FD5** compounds after **FCO-2FR1**. Whereas, the other derivatives showed minute spots of electronic charge shift in the acceptor part. Overall, most of the charge is localized in the π-spacer region in all compounds and is minutely transferred towards the acceptor region. Furthermore, a significant coherence of charge is seen in both diagonal and off-diagonal elements in the derivatives.

3.8. Exciton binding energies (E_b)

Binding energy (E_b) is a crucial factor in determining the rate of charge separation and optoelectronic properties of compound. It shows a direct relationship with energy gap and optimization energy values, while, shows an inverse relation with the exciton dissociation and charge mobilities. The lower E_b shows the higher exciton dissociation in compounds and vice-versa. It can be determined by subtracting the E_{gap} from the energy of optimization [66,67] and is represented by Equation (9).

$$E_b = E_{L-H} - E_{opt} \quad \text{(Equation 9)}$$

Here, E_b is denoted as the binding energy, E_{opt} is the first excitation energy and $E_{L\text{-}H}$ is energy band gap [68].

Interestingly, all the designed chromophores (**FD2-FD6**) exhibited lower E_b values than **FCO-2FR1** (see Table 6). Moreover, they also showed lesser values than 1.9 eV and indicated higher exciton dissociation rate with larger rate of charge transfer which is essential for perfect photonic and nonlinear response [69]. The following decreasing trend of binding energy (in *eV*) is observed in the investigated series of compounds: **FCO-2FR1** (0.309) > **FD5** (0.210) > **FD4** (0.196) > **FD6** (0.031) > **FD3** (-0.338) > **FD2** (-0.432).

From the facts obtained *via* transition heat maps and associated E_b values for the series of compounds under discussion, we have come to the conclusion that proposed tailored compounds are better candidates for NLO as they showed efficient allocation of charges from donor towards acceptor moiety.

3.9. Natural population analysis (NPA)

The charge dissemination on an atom had a great impact on the dipole moment, chemical reactivity and electrostatic interaction between the atoms and molecules and many other properties of the chemical system. The natural population analysis determines the electronic charge transformation and electrostatic potential on the external surface of molecules under study [70]. The electronic charge plays a key role towards the substantial contribution in the molecular conformation and bonding patterns [71]. The effective calculation of atomic charge of the reference (**FCO-2FR1**) and the designed compounds (**FD2-FD6**) is significant for the better understanding of their molecular system [72,73].The dissemination of charges describe that the nitrogen atoms associated with oxygen in all compounds are negatively charged, while, the sulfur atoms are positively charged (see Fig. S15). Furthermore, all the hydrogen atoms are also positively charged in **FCO-2FR1** and **FD2-FD6** compounds. Natural population investigation shows that no inconsistency in charge distribution is found over all the hydrogen atoms. Some of the carbon atoms are negatively charged, while, some are positively charged due to its donating and accepting nature of electrons, respectively. The inclusive investigation of NBO charges revealed that the unequal distribution of charges on the designed compounds is due to the nitrogen and oxygen atoms.

3.10. Nonlinear optical properties

The nonlinear properties are associated with several high-tech applications such as telecommunication, laser frequency modulation and biomedicine for which their study is crucial both at molecular and bulk levels [74,75,76]. The electrical properties of compound determine their nonlinear characteristics such as polarizability (linear response) and hyper-polarizability (non-linear response). For

Table 6
Computed binding energy (E_b) of entitled chromophores.

Compounds	$E_{L\text{-}H}$	E_{opt}	E_b
FCO-2FR1	2.052	1.743	0.309
FD2	1.223	1.655	-0.432
FD3	1.309	1.647	-0.338
FD4	1.725	1.529	0.196
FD5	1.774	1.564	0.210
FD6	1.611	1.580	0.0310

Units in *eV*.

this reason, both the polarizability and hyper-polarizability are assessed to estimate linear and NLO potential of materials. Generally, a linear polarizability is essential to obtain large hyperpolaizability [77]. It is also well known that NLO response is exhibited by non-centrosymmetric materials. Therefore, the electronic spatial extent is considered as a prototype of push-pull chromophores (Donor-π-Acceptor).

The organic compounds are the preferred candidates which possess substantial features which effectively deal with the light-matter interactions [78]. Moreover, the push-pull mechanisms of organic chromophores are influenced due to the presence of π–conjugation feature in compounds, generating higher magnitudes of NLO properties. The NLO properties are determined using quantum chemical methods *via* the parameters such as dipole moment (μ_{tot}) [79], linear polarizability $\langle\alpha\rangle$ [80] and first hyper-polarizability (β_{tot}) [81]. The reported structural modifications enhanced not only the charge transference (due to lower band gaps) but also the linear and hyper-polarizability values, highly associated with NLO response properties. The μ_{tot}, $\langle\alpha\rangle$ and β_{tot} are calculated for the investigated molecules (**FCO-2FR1** and **FD2-FD6**) using Equations 10–15. Moreover, Equations (12a)-12c) shows the tensors of hyperpolarizability along three axis (x, y and z).

$$\mu = \left(\mu_x^2 + \mu_y^2 + \mu_z^2\right)^{1/2} \quad \text{(Equation 10)}$$

$$\langle\alpha\rangle = 1/3\left(\alpha_{xx} + \alpha_{yy} + \alpha_{zz}\right) \quad \text{(Equation 11)}$$

$$\beta\_(\text{tot}) = \left(\beta_x^2 + \beta_y^2 + \beta_z^2\right)^{1}/^{2} \quad \text{(Equation 12)}$$

$$\beta_x = \beta_{xxx+}\beta_{xyy+}\beta_{xzz} \quad \text{(Equation 12a)}$$

$$\beta_y = \beta_{yxx+}\beta_{yyy+}\beta_{yzz} \quad \text{(Equation 12b)}$$

$$\beta_z = \beta_{zxx+}\beta_{zyy+}\beta_{zzz} \quad \text{(Equation 12c)}$$

Where, μ_{tot} is in Debye (*D*) and $\langle\alpha\rangle$, β_{tot} are in *esu*.

3.10.1. Dipole polarizability

The dipole moment or dipole polarizability (*u*) is defined as the factor highly influenced by electronegativity difference and is obtained as a product of magnitude of charges and the distance between them. The larger electronegativity indicate the higher dipole moment values in a system [82]. Moreover, the polarity along with the dipole moment plays a key role in enhancing the nonlinear properties of a molecule [83]. The u_{tot} is called as the average dipole moment, while, u_x, u_y and u_z are known as the contributing tensors along x, y and z-orientations which determine the u_{tot} [84]. Their values are calculated in debye (*D*), recorded in Table S20, while, the major u_{tot} values are presented in the manuscript (Table 7). The extraordinary high u_{tot} are observed in designed derivatives (**FD2-FD6**) *i.e.,* in the range of 11.175–20.049 *D* as compared to **FCO-2FR1** with $u_{tot} = 4.065$ *D*. The following decreasing order is obtained in the entitled chromophores: **FD2 > FD3 > FD5 > FD4 > FD6 > FCO-2FR1**. The results showed that y-axis is majorly contributing in the average values of dipole moment more than x- and z-axes (see Table S20). The **FD2** compound is found as the most polarizable molecule with highest $u_{tot} = 20.049$ *D* with contributing tensors calculated as $u_x = -19.998$ *D*, $u_y =$ -1.393 and $u_z = 0.346$ *D*. The dipole moment of urea is considered as a standard value for comparison, recorded as 1.373 *D* in the literature [58]. Fortunately, our designed compounds showed much larger dipole moments than urea.

3.10.2. Linear polarizability

The linear polarizability $\langle\alpha\rangle$ (also known as first-order NLO response) is related with intramolecular charge transfer (ICT) which operates from D *via* π–linkers towards the A species. The external electrical field interacts with the excess electrons in such systems and enhance the dipole moments which in turn increase the linear polarizability and first-order hyper-polarizability [85]. Table S21 shows the $\langle\alpha\rangle$ value for compounds under discussion (**FCO-2FR1** and **FD2-FD6**) and also revealed the important 3-*D* tensors for polarizability. For **FCO-2FR1**, the $\langle\alpha\rangle = 2.318 \times 10^{-22}$ *esu* which is known as the lowermost value in the recorded series of compounds. The **FD3** has shown the most polarizable nature with significantly highest $\langle\alpha\rangle = 2.936 \times 10^{-22}$ *esu*. The rest of the molecules (**FD2**, **FD4**, **FD5** and **FD6**) have shown $\langle\alpha\rangle$ values as 2.618×10^{-22}, 2.850×10^{-22}, 2.879×10^{-22} and 2.811×10^{-22} *esu*, respectively. Similarly, a detailed study of their related tensors (α_{xx}, α_{yy} and α_{zz}) predicts the $\langle\alpha\rangle$ values which demonstrated that α_{xx} is the major contributing tensor for

Table 7
The computed NLO properties for **FCO-2FR1** and **FD2-FD6**.

Systems	μ_{tot}	$\langle\alpha\rangle \times 10^{-22}$	$\beta_{tot} \times 10^{-27}$
FCO-2FR1	4.065	2.318	0.7724
FD2	20.049	2.618	11.22
FD3	19.055	2.936	8.223
FD4	12.138	2.850	4.661
FD5	12.420	2.879	4.384
FD6	11.175	2.811	4.215

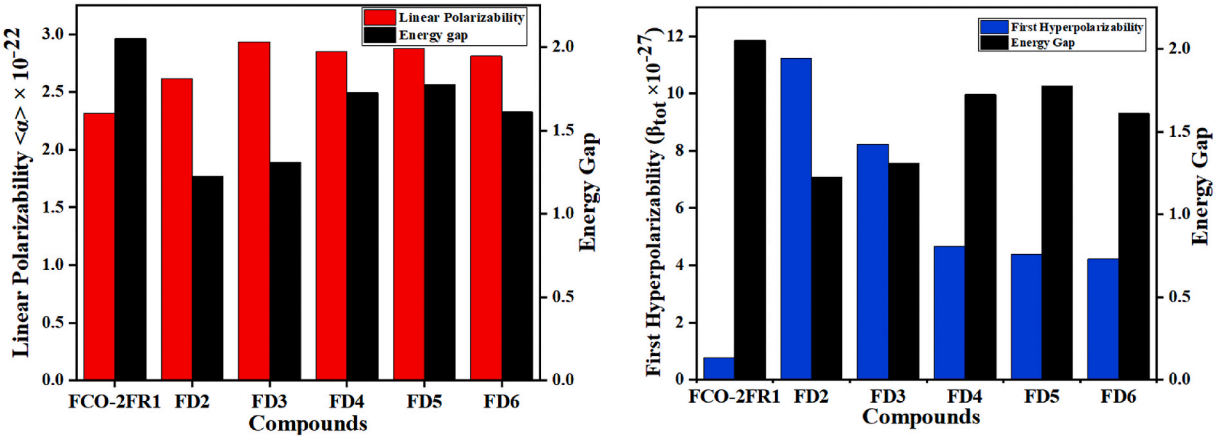

Fig. 8. A comparison of energy gaps with $\langle\alpha\rangle$ and β_{tot} for entitled chromophores.

linear polarizability in compounds. All the entitled compounds have shown comparable values of $\langle\alpha\rangle$ with the following decreasing trend: **FD3 > FD5 > FD4 > FD6 > FD2 > FCO-2FR1**.

3.10.3. First hyper-polarizability

The first hyper-polarizability (β_{tot}) is profoundly a contributing factor in calculating the NLO response of a compound [86]. It is increased in the presence of excessively strong push-pull models which take part in enhancing the molecular nonlinearity owing to the extended conjugation [87]. The values are determined which contain nine contributing tensors listed as β_{xxx}, β_{xxy}, β_{xyy}, β_{yyy}, β_{xxz}, β_{yyz}, β_{xzz}, β_{yzz}, β_{zzz}. The detailed hyper-polarizability results are tabulated in Table S22, whereas, the average values of β_{tot} are also recorded in Table 7. A linear decreasing trend is observed in the values among the investigated compounds (**FD3-FD6**) *i.e.,* (**FD3** = 8.223 × 10^{-27}, **FD4** = 4.661 × 10^{-27}, **FD5** = 4.384 × 10^{-27}, **FD6** = 4.215 × 10^{-27}). Whereas, the compound (**FD2**) possesses the highest *i.e.,* 11.22 × 10^{-27} *esu* and **FCO-2FR1** has shown the least β_{tot} value as 0.7724 × 10^{-27} *esu*. Further, the results of β_{tot} are also compared with first hyper-polarizability of urea molecule (β_{tot} = 0.372 × 10^{-30} *esu*) [88]. The comparison shows that **FCO-2FR1** exhibited 2.076 × 10^{-57} times higher β_{tot} than the standard urea molecule. Similarly, for **FD2** (3.016 × 10^{-56}), **FD3** (2.210 × 10^{-56}), **FD4** (1.253 × 10^{-56}), **FD5** (1.178 × 10^{-56}) and **FD6** (1.133 × 10^{-56}) times higher values are observed.

The graphical representation further illustrates the correspondence of $\langle\alpha\rangle$ and β_{tot} results with HOMO-LUMO energy gaps for the studied compounds (Fig. 8). The depicted NLO properties showed that the **FD2** molecule possessed the highest dipole moment (20.049 *D*) and first hyper-polarizability values (8.223 × 10^{-27} *esu*) and **FD3** has shown the highest linear polarizability value (2.936 × 10^{-22} *esu*). The reason might be their reduced energy gaps *i.e.,*1.223 and 1.308 eV, respectively. Furthermore, they possess the higher values of global softness (σ) as 0.817 and 0.765 eV, respectively which clearly depicts that the soft molecules are more polarizable than hard molecules. Thus, the investigated organic chromophores are regarded as the suitable materials with potential NLO amplitudes. Moreover, it has been observed in this study that suitable donor species could play a significant role in determining the NLO response among the π–conjugated systems.

4. Conclusion

In summary, we have systematically designed new molecular entities (**FD2-FD6**) with D–π–A architecture from the non-fullerene acceptor molecule (**FCO-2FR1**). The DFT/TDDFT calculations have been performed to elucidate the relation among D, π–spacer and A moiety in the designed push-pull schemes. Surprisingly, all the compounds (**FD2-FD6**) exhibited a prominent decrease in their HOMO-LUMO energy gap as compared to the **FCO-2FR1** molecule. The least band gap is obtained in case of **FD2** compound as 1.223 eV. Similarly, their UV–Vis spectra were reported to have a prominent bathochromic shift with correspondingly smaller transition energies. Furthermore, the NBOs investigation depicts their stability due to intramolecular interactions and formation of charge separation states. Here also, the highest stabilization energy is exhibited by **FD2** (28.40 kcal mol^{-1}). The tailored species showed lower binding energies (E_b) from the reference compound and offered less Coulombic force which also influenced their TDM heat maps. Overall, a significant charge transfer is observed from D towards A *via* the π–spacer among the designed molecules. Interestingly, an eye-catching NLO response is seen in **FD2-FD6** as compared to **FCO-2FR1**. Among the designed species, the highest β_{tot} and u_{tot} are obtained for **FD2** *i.e.*, 11.22 × 10^{-27} *esu* and 20.049 *D*, respectively, whereas, the largest $\langle\alpha\rangle$ is 2.936 × 10^{-22} *esu* observed in case of **FD3**. Also, their GRP studies proved them as the softest molecules with σ values as 0.817 and 0.765 eV, respectively. Expectedly, the two compounds (**FD2** and **FD3**) also exhibited the least E_b values as -0.432 and -0.338 eV, respectively, which indicate the higher exciton dissociation rate and support their large NLO response properties. Consequently, **FD2** and **FD3** are preferred as better NLO entrants for the future. The present study also emphasizes the role of donor species in the fine-tuning of NLO attributes. Therefore, this research work would provide the experimentalists an enrich understanding of structure-property relationships of designed compounds and would also pave a pathway in their synthesis for reasonable NLO response.

Author contribution statement

Muhammad Khalid, Mashal Khan: Conceived and designed the experiments; Wrote the paper. Iqra Shafiq, Khalid Mahmood: Performed the experiments; Wrote the paper. Muhammad Nadeem Akhtar, Javed Iqbal: Analyzed and interpreted the data; Wrote the paper. Mohammad Khalid Al-Sadoon, Wajid Zaman, Ataualpa Albert Carmo Braga: Contributed reagents, materials, analysis tools or data; Wrote the paper.

Funding statement

The authors would like to extend their sincere appreciation to the Researchers Supporting Project Number (RSP2023R410), King Saud University, Riyadh, Saudi Arabia.

Data availability statement

Data included in article/supplementary material/referenced in article.

Declaration of competing interest

The authors declare no competing interests.

Appendix B. Supplementary data

Supplementary data related to this article can be found at https://doi.org/10.1016/j.heliyon.2023.e13033.

References

[1] B. Sivasankari, S.M. Roopan, L-Malic acid-doped Guanidinium Carbonate crystal: a New NLO Material and its photoluminescence study, Optik 226 (2021), 165909.
[2] N. Kosar, K. Ayub, T. Mahmood, Surface functionalization of twisted graphene C32H15 and C104H52 derivatives with alkalis and superalkalis for NLO response; a DFT study, J. Mol. Graph. Model. 102 (2021), 107794.
[3] S. Vasumathi, H.J. Jeyakumar, P. Selvarajan, Spectral, NLO, thermal, hardness and SEM studies of phosphate doped bis-urea oxalic acid crystals for laser applications, Chin. J. Phys. 73 (2021) 1–12.
[4] R.-L. Zhong, H.-L. Xu, S. Muhammad, J. Zhang, Z.-M. Su, The stability and nonlinear optical properties: encapsulation of an excess electron compound LiCN··· Li within boron nitride nanotubes, J. Mater. Chem. 22 (2012) 2196–2202.
[5] A. Ahsin, K. Ayub, Remarkable electronic and NLO properties of bimetallic superalkali clusters: a DFT study, J. Nanostruct. Chem. (2021) 1–17.
[6] B. Khan, M. Khalid, M.R. Shah, M.N. Tahir, H.M. Asif, H.A.R. Aliabad, A. Hussain, Synthetic, spectroscopic, SC-XRD and nonlinear optical analysis of potent hydrazide derivatives: a comparative experimental and DFT/TD-DFT exploration, J. Mol. Struct. 1200 (2020), 127140.
[7] M.U. Khan, M. Khalid, M. Ibrahim, A.A.C. Braga, M. Safdar, A.A. Al-Saadi, M.R.S.A. Janjua, First theoretical framework of triphenylamine–dicyanovinylene-based nonlinear optical dyes: structural modification of π-linkers, J. Phys. Chem. C 122 (2018) 4009–4018.
[8] M.U. Khan, M. Ibrahim, M. Khalid, M.S. Qureshi, T. Gulzar, K.M. Zia, A.A. Al-Saadi, M.R.S.A. Janjua, First theoretical probe for efficient enhancement of nonlinear optical properties of quinacridone based compounds through various modifications, Chem. Phys. Lett. 715 (2019) 222–230.
[9] M.R.S.A. Janjua, C.-G. Liu, W. Guan, J. Zhuang, S. Muhammad, L.-K. Yan, Z.-M. Su, Prediction of remarkably large second-order nonlinear optical properties of organoimido-substituted hexamolybdates, J. Phys. Chem. 113 (2009) 3576–3587.
[10] D.R. Kanis, M.A. Ratner, T.J. Marks, Design and construction of molecular assemblies with large second-order optical nonlinearities. Quantum chemical aspects, Chem. Rev. 94 (1994) 195–242.
[11] S.K. Hurst, N.T. Lucas, M.G. Humphrey, I. Asselberghs, R. Van Boxel, A. Persoons, Organometallic complexes for non-linear optics. XXVI. Quadratic hyperpolarizabilities of some 4-methoxytetrafluorophenylalkynyl gold and ruthenium complexes, Aust. J. Chem. 54 (2001) 447–451.
[12] T. Sivakumar, S. Vignesh, K.S. Jeyaperumal, A.L. Muppudathi, Synthesis, growth and investigation of structural, optical, photoluminescence and thermal studies on the ZnSO4-doped DAST crystal for NLO applications, J. Mater. Sci. Mater. Electron. 32 (2021) 17936–17945.
[13] D.J. Williams, Non-linear optical properties of organic materials, Thin Solid Films 216 (1992) 117–122.
[14] S.-J. Kim, B.J. Kang, U. Puc, W.T. Kim, M. Jazbinsek, F. Rotermund, O.-P. Kwon, Highly nonlinear optical organic crystals for efficient terahertz wave generation, detection, and applications, Adv. Opt. Mater. 9 (2021), 2101019.
[15] Y. Atalay, D. Avcı, A. Başoğlu, Linear and non-linear optical properties of some donor–acceptor oxadiazoles by ab initio Hartree-Fock calculations, Struct. Chem. 19 (2008) 239–246.
[16] R. Mahmood, M.R.S.A. Janjua, S. Jamil, DFT molecular simulation for design and effect of core bridging acceptors (BA) on NLO response: first theoretical framework to enhance nonlinearity through BA, J. Cluster Sci. 28 (2017) 3175–3183.
[17] M. Khalid, M.U. Khan, I. Shafiq, R. Hussain, A. Ali, M. Imran, A.A. Braga, M. Fayyaz ur Rehman, M.S. Akram, Structural Modulation of π-conjugated Linkers in D–π–A Dyes Based on Triphenylamine Dicyanovinylene Framework to Explore the NLO Properties, vol. 8, Royal Society Open Science, 2021, 210570.
[18] S.P. Singh, Impact of end groups on the performance of non-fullerene acceptors for organic solar cell applications, J. Mater. Chem. 7 (2019) 22701–22729.
[19] J. Hou, O. Inganäs, R.H. Friend, F. Gao, Organic solar cells based on non-fullerene acceptors, Nat. Mater. 17 (2018) 119–128.
[20] L. Duan, N.K. Elumalai, Y. Zhang, A. Uddin, Progress in non-fullerene acceptor based organic solar cells, Sol. Energy Mater. Sol. Cell. 193 (2019) 22–65.
[21] L. Yang, M. Li, J. Song, Y. Zhou, Z. Bo, H. Wang, Molecular consideration for small molecular acceptors based on ladder-type dipyran: influences of O-functionalization and π-bridges, Adv. Funct. Mater. 28 (2018), 1705927.
[22] A. Mahmood, J. Yang, J. Hu, X. Wang, A. Tang, Y. Geng, Q. Zeng, E. Zhou, Introducing four 1, 1-dicyanomethylene-3-indanone end-capped groups as an alternative strategy for the design of small-molecular nonfullerene acceptors, J. Phys. Chem. C 122 (2018) 29122–29128.
[23] M.U. Khan, M. Khalid, R. Hussain, A. Umar, M.Y. Mehboob, Z. Shafiq, M. Imran, A. Irfan, Novel W-shaped oxygen heterocycle-fused fluorene-based non-fullerene acceptors: first theoretical framework for designing environment-friendly organic solar cells, Energy Fuels 35 (2021) 12436–12450.

[24] N. Boukabcha, A. Djafri, Y. Megrouss, Ö. Tamer, D. Avcı, M. Tuna, N. Dege, A. Chouaih, Y. Atalay, F. Hamzaoui, Synthesis, crystal structure, spectroscopic characterization and nonlinear optical properties of (Z)-N'-(2, 4-dinitrobenzylidene)-2-(quinolin-8-yloxy) acetohydrazide, J. Mol. Struct. 1194 (2019) 112–123.
[25] N. Dege, H. Gökce, O.E. Doğan, G. Alpaslan, T. Ağar, S. Muthu, Y. Sert, Quantum computational, spectroscopic investigations on N-(2-((2-chloro-4, 5-dicyanophenyl) amino) ethyl)-4-methylbenzenesulfonamide by DFT/TD-DFT with different solvents, molecular docking and drug-likeness researches, Colloids Surf. A Physicochem. Eng. Asp. 638 (2022), 128311.
[26] S. Demir, S. Cakmak, N. Dege, H. Kutuk, M. Odabasoglu, R.A. Kepekci, A novel 3-acetoxy-2-methyl-N-(4-methoxyphenyl) benzamide: molecular structural describe, antioxidant activity with use X-ray diffractions and DFT calculations, J. Mol. Struct. 1100 (2015) 582–591.
[27] S. Demir, F. Tinmaz, N. Dege, I.O. Ilhan, Vibrational spectroscopic studies, NMR, HOMO–LUMO, NLO and NBO analysis of 1-(2-nitrobenzoyl)-3, 5-diphenyl-4, 5-dihydro-1H-pyrazole with use X-ray diffractions and DFT calculations, J. Mol. Struct. 1108 (2016) 637–648.
[28] M.K. Gümüş, S. Kansız, E. Aydemir, N.Y. Gorobets, N. Dege, Structural features of 7-methoxy-5-methyl-2-(pyridin-3-yl)-11, 12-dihydro-5, 11-methano [1, 2, 4] triazolo [1, 5-c][1, 3, 5] benzoxadiazocine: experimental and theoretical (HF and DFT) studies, surface properties (MEP, Hirshfeld), J. Mol. Struct. 1168 (2018) 280–290.
[29] D.S. Sholl, J.A. Steckel, Density Functional Theory: A Practical Introduction, John Wiley & Sons, 2011.
[30] M.J. Frisch, G.W. Trucks, H.B. Schlegel, G.E. Scuseria, M.A. Robb, J.R. Cheeseman, G. Scalmani, V. Barone, G.A. Petersson, H. Nakatsuji, Gaussian 09 Reference. Gaussian 09, Revision A. 02, Gaussian, Inc., Wallingford CT, 2016.
[31] M.R.S.A. Janjua, M. Haroon, R. Hussain, M. Usman, M.U. Khan, W.A. Gill, Computational engineering to enhance the photovoltaic by end-capped and bridging core alterations: empowering the future with solar energy through synergistic effect in D-A materials, Int. J. Quant. Chem. 122 (2022), e26821.
[32] S.B. Numbury, Designing of small organic non-fullerene (NFAs) acceptor molecules with an A- D- A framework for high-performance organic solar cells: a DFT and TD-DFT method, Oxford Open Materials Science 2 (2022), itac002.
[33] E. Nazarparvar, M. Zahedi, E. Klein, Density functional theory (B3LYP) study of substituent effects on O–H bond dissociation enthalpies of trans-resveratrol derivatives and the role of intramolecular hydrogen bonds, J. Org. Chem. 77 (2012) 10093–10104.
[34] R.D. Dennington, T.A. Keith, J.M. Millam, GaussView 5.0, Gaussian, Inc., Wallingford, 2008, p. 20.
[35] A.L. Tenderholt, PyMOlyze, 2007, Version 2.0.
[36] F. Weinhold, E.D. Glendening, NBO 5.0 Program Manual: Natural Bond Orbital Analysis Programs, Theoretical Chemistry Institute and Department of Chemistry, University of Wisconsin, Madison, WI, 2001, 53706.
[37] M.D. Hanwell, D.E. Curtis, D.C. Lonie, T. Vandermeersch, E. Zurek, G.R. Hutchison, Avogadro: an advanced semantic chemical editor, visualization, and analysis platform, J. Cheminf. 4 (2012) 1–17.
[38] G.A. Zhurko, Chemcraft, 2014. Received: October. 22.
[39] N.M. O'Boyle, GaussSum (2007), Version 2.0. 5.
[40] J.C. Kromann, C. Steinmann, J.H. Jensen, Improving solvation energy predictions using the SMD solvation method and semiempirical electronic structure methods, J. Chem. Phys. 149 (2018), 104102.
[41] A. Plaquet, M. Guillaume, B. Champagne, F. Castet, L. Ducasse, J.-L. Pozzo, V. Rodriguez, In silico optimization of merocyanine-spiropyran compounds as second-order nonlinear optical molecular switches, Phys. Chem. Chem. Phys. 10 (2008) 6223–6232.
[42] X. Ke, L. Meng, X. Wan, Y. Sun, Z. Guo, S. Wu, H. Zhang, C. Li, Y. Chen, An oxygen heterocycle-fused fluorene based non-fullerene acceptor for high efficiency organic solar cells, Mater. Chem. Front. 4 (2020) 3594–3601.
[43] A. Mahmood, M.I. Abdullah, S.U.-D. Khan, Enhancement of nonlinear optical (NLO) properties of indigo through modification of auxiliary donor, donor and acceptor, Spectrochim. Acta Mol. Biomol. Spectrosc. 139 (2015) 425–430.
[44] S. Uzun, Z. Esen, E. Koç, N.C. Usta, M. Ceylan, Experimental and density functional theory (MEP, FMO, NLO, Fukui functions) and antibacterial activity studies on 2-amino-4-(4-nitrophenyl)-5, 6-dihydrobenzo [h] quinoline-3-carbonitrile, J. Mol. Struct. 1178 (2019) 450–457.
[45] K. Ayub, Are phosphide nano-cages better than nitride nano-cages? A kinetic, thermodynamic and non-linear optical properties study of alkali metal encapsulated X 12 Y 12 nano-cages, J. Mater. Chem. C 4 (2016) 10919–10934.
[46] M.U. Khan, M. Khalid, I. Shafiq, R.A. Khera, Z. Shafiq, R. Jawaria, M. Shafiq, M.M. Alam, A.A.C. Braga, M. Imran, Theoretical investigation of nonlinear optical behavior for rod and T-Shaped phenothiazine based D-π-A organic compounds and their derivatives, J. Saudi Chem. Soc. 25 (2021), 101339.
[47] S. Katariya, L. Rhyman, I.A. Alswaidan, P. Ramasami, N. Sekar, Triphenylamine-based fluorescent styryl dyes: DFT, TD-DFT and non-linear optical property study, J. Fluoresc. 27 (2017) 993–1007.
[48] M. Ans, J. Iqbal, Z. Ahmad, S. Muhammad, R. Hussain, B. Eliasson, K. Ayub, Designing three-dimensional (3D) non-fullerene small molecule acceptors with efficient photovoltaic parameters, ChemistrySelect 3 (2018) 12797–12804.
[49] V. Barone, M. Cossi, Quantum calculation of molecular energies and energy gradients in solution by a conductor solvent model, J. Phys. Chem. 102 (1998) 1995–2001.
[50] W. Rahmalia, J.-F. Fabre, T. Usman, Z. Mouloungui, Aprotic solvents effect on the UV–visible absorption spectra of bixin, Spectrochim. Acta Mol. Biomol. Spectrosc. 131 (2014) 455–460.
[51] M.D. Adeoye, A.I. Adeogun, S. Adewuyi, S.A. Ahmed, N.W. Odozi, N.O. Obi-Egbeedi, Effect of solvents on the electronic absorption spectra of 9, 14 dibenzo (a,c) phenazine and tribenzo (a, c,i) phenazine, Sci. Res. Essays 4 (2009) 107–111.
[52] T. Koopmans, Über die Zuordnung von Wellenfunktionen und Eigenwerten zu den einzelnen Elektronen eines Atoms, Physica 1 (1934) 104–113.
[53] R.G. Parr, R.A. Donnelly, M. Levy, W.E. Palke, Electronegativity: the density functional viewpoint, J. Chem. Phys. 68 (1978) 3801–3807.
[54] P.K. Chattaraj, D.R. Roy, Update 1 of: electrophilicity index, Chem. Rev. 107 (2007) PR46–PR74.
[55] R.G. Pearson, Absolute electronegativity and hardness correlated with molecular orbital theory, Proc. Natl. Acad. Sci. USA 83 (1986) 8440–8441.
[56] R.G. Parr, R.G. Pearson, Absolute hardness: companion parameter to absolute electronegativity, J. Am. Chem. Soc. 105 (1983) 7512–7516.
[57] M.N. Tahir, M. Khalid, A. Islam, S.M.A. Mashhadi, A.A. Braga, Facile synthesis, single crystal analysis, and computational studies of sulfanilamide derivatives, J. Mol. Struct. 1127 (2017) 766–776.
[58] M. Khalid, A. Ali, R. Jawaria, M.A. Asghar, S. Asim, M.U. Khan, R. Hussain, M.F. ur Rehman, C.J. Ennis, M.S. Akram, First principles study of electronic and nonlinear optical properties of A–D–π–A and D–A–D–π–A configured compounds containing novel quinoline–carbazole derivatives, RSC Adv. 10 (2020) 22273–22283.
[59] R.G. Pearson, The electronic chemical potential and chemical hardness, J. Mol. Struct.: THEOCHEM 255 (1992) 261–270.
[60] E.D. Glendening, C.R. Landis, F. Weinhold, Natural bond orbital methods, Wiley Interdiscip. Rev. Comput. Mol. Sci. 2 (2012) 1–42.
[61] K.G. Krishnan, R. Sivakumar, V. Thanikachalam, H. Saleem, Synthesis, spectroscopic investigation and computational study of 3-(1-(((methoxycarbonyl) oxy) imino) ethyl)-2H-chromen-2-one, Spectrochim. Acta Mol. Biomol. Spectrosc. 144 (2015) 29–42.
[62] R. Hussain, M.U. Khan, M.Y. Mehboob, M. Khalid, J. Iqbal, K. Ayub, M. Adnan, M. Ahmed, K. Atiq, K. Mahmood, Enhancement in photovoltaic properties of N, N-diethylaniline based donor materials by bridging core modifications for efficient solar cells, ChemistrySelect 5 (2020) 5022–5034.
[63] L. Wang, J.-T. Ye, H.-Q. Wang, H.-M. Xie, Y.-Q. Qiu, Self-assembled donor–acceptor chromophores: evident layer effect on the first hyperpolarizability and two-dimensional charge transfer character, J. Phys. Chem. C 121 (2017) 21616–21626.
[64] M.U. Khan, R. Hussain, M. Yasir Mehboob, M. Khalid, Z. Shafiq, M. Aslam, A.A. Al-Saadi, S. Jamil, M.R.S.A. Janjua, In silico modeling of new "Y-Series"-based near-infrared sensitive non-fullerene acceptors for efficient organic solar cells, ACS Omega 5 (2020) 24125–24137.
[65] T. Lu, F. Chen, Multiwfn: a multifunctional wavefunction analyzer, J. Comput. Chem. 33 (2012) 580–592.
[66] S. Kraner, G. Prampolini, G. Cuniberti, Exciton binding energy in molecular triads, J. Phys. Chem. C 121 (2017) 17088–17095.
[67] M. Naeem, S. Jabeen, R.A. Khera, U. Mubashar, J. Iqbal, Tuning of optoelectronic properties of triphenylamines-based donor materials for organic solar cells, J. Theor. Comput. Chem. 18 (2019), 1950036.
[68] A. Mahmood, A. Irfan, Effect of fluorination on exciton binding energy and electronic coupling in small molecule acceptors for organic solar cells, Comput. Theoretical Chem. 1179 (2020), 112797.

[69] M. Khalid, M.U. Khan, E. Razia, Z. Shafiq, M.M. Alam, M. Imran, M.S. Akram, Exploration of efficient electron acceptors for organic solar cells: rational design of indacenodithiophene based non-fullerene compounds, Sci. Rep. 11 (2021) 1–15.
[70] R.S. Mulliken, Electronic population analysis on LCAO–MO molecular wave functions. I, J. Chem. Phys. 23 (1955) 1833–1840.
[71] R.G. Parr, R.G. Pearson, Absolute hardness: companion parameter to absolute electronegativity, J. Am. Chem. Soc. 105 (1983) 7512–7516.
[72] Z. Demircioğlu, G. Kaştaş, Ç.A. Kaştaş, R. Frank, Spectroscopic, XRD, Hirshfeld surface and DFT approach (chemical activity, ECT, NBO, FFA, NLO, MEP, NPA& MPA) of (E)-4-bromo-2-[(4-bromophenylimino) methyl]-6-ethoxyphenol, J. Mol. Struct. 1191 (2019) 129–137.
[73] Z. Demircioğlu, Ç.A. Kaştaş, O. Büyükgüngör, X-ray structural, spectroscopic and computational approach (NBO, MEP, NLO, NPA, fukui function analyses) of (E)-2-((4-bromophenylimino) methyl)-3-methoxyphenol, Mol. Cryst. Liq. Cryst. 656 (2017) 169–184.
[74] I. Sheikhshoaie, W.M. Fabian, Quantum chemical study on the electronic structure and second-order nonlinear optical properties of salen-type Schiff bases, Dyes Pigments 70 (2006) 91–98.
[75] A. Iwan, D. Sek, Polymers with triphenylamine units: photonic and electroactive materials, Prog. Polym. Sci. 36 (2011) 1277–1325.
[76] S.N. Margar, N. Sekar, Nonlinear optical properties of curcumin: solvatochromism-based approach and computational study, Mol. Phys. 114 (2016) 1867–1879.
[77] C. Qin, A.E. Clark, DFT characterization of the optical and redox properties of natural pigments relevant to dye-sensitized solar cells, Chem. Phys. Lett. 438 (2007) 26–30.
[78] J. Deb, D. Paul, U. Sarkar, Density functional theory investigation of nonlinear optical properties of T-graphene quantum dots, J. Phys. Chem. 124 (2020) 1312–1320.
[79] J.-L. Oudar, D.S. Chemla, Hyperpolarizabilities of the nitroanilines and their relations to the excited state dipole moment, J. Chem. Phys. 66 (1977) 2664–2668.
[80] A. Alparone, Linear and nonlinear optical properties of nucleic acid bases, Chem. Phys. 410 (2013) 90–98.
[81] A. Plaquet, M. Guillaume, B. Champagne, F. Castet, L. Ducasse, J.-L. Pozzo, V. Rodriguez, In silico optimization of merocyanine-spiropyran compounds as second-order nonlinear optical molecular switches, Phys. Chem. Chem. Phys. 10 (2008) 6223–6232.
[82] K. Fukui, Role of frontier orbitals in chemical reactions, Science 218 (1982) 747–754.
[83] A. Saeed, S. Muhammad, S. Rehman, S. Bibi, A.G. Al-Sehemi, M. Khalid, Exploring the impact of central core modifications among several push-pull configurations to enhance nonlinear optical response, J. Mol. Graph. Model. 100 (2020), 107665.
[84] K.J. Miller, Calculation of the molecular polarizability tensor, J. Am. Chem. Soc. 112 (1990) 8543–8551.
[85] M. Ahn, M.-J. Kim, D.W. Cho, K.-R. Wee, Electron push–pull effects on intramolecular charge transfer in perylene-based donor–acceptor compounds, J. Org. Chem. 86 (2020) 403–413.
[86] T.J. Marks, M.A. Ratner, Design, synthesis, and properties of molecule-based assemblies with large second-order optical nonlinearities, Angew Chem. Int. Ed. Engl. 34 (1995) 155–173.
[87] D.R. Kanis, M.A. Ratner, T.J. Marks, Design and construction of molecular assemblies with large second-order optical nonlinearities. Quantum chemical aspects, Chem. Rev. 94 (1994) 195–242.
[88] S.N. Margar, N. Sekar, Nonlinear optical properties of curcumin: solvatochromism-based approach and computational study, Mol. Phys. 114 (2016) 1867–1879.